Evaluation of the Surface Representation of the Greenland Ice Sheet in a General Circulation Model

RICHARD I. CULLATHER

Earth System Science Interdisciplinary Center, University of Maryland, College Park, College Park, Maryland

SOPHIE M. J. NOWICKI

Cryospheric Sciences Laboratory, NASA Goddard Space Flight Center, Greenbelt, Maryland

BIN ZHAO

Science Applications International Corporation, Greenbelt, Maryland

MAX J. SUAREZ

Global Modeling and Assimilation Office, NASA Goddard Space Flight Center, Greenbelt, Maryland

(Manuscript received 17 October 2013, in final form 24 February 2014)

ABSTRACT

Simulated surface conditions of the Goddard Earth Observing System model, version 5 (GEOS-5), atmospheric general circulation model (AGCM) are examined for the contemporary Greenland Ice Sheet (GrIS). A surface parameterization that explicitly models surface processes including snow compaction, meltwater percolation and refreezing, and surface albedo is found to remedy an erroneous deficit in the annual net surface energy flux and provide an adequate representation of surface mass balance (SMB) in an evaluation using simulations at two spatial resolutions. The simulated 1980–2008 GrIS SMB average is 24.7 ± 4.5 cm yr^{-1} water-equivalent (w.e.) at ½° model grid spacing, and 18.2 ± 3.3 cm yr^{-1} w.e. for 2° grid spacing. The spatial variability and seasonal cycle of the ½° simulation compare favorably to recent studies using regional climate models, while results from 2° integrations reproduce the primary features of the SMB field. In comparison to historical glaciological observations, the coarser-resolution model overestimates accumulation in the southern areas of the GrIS, while the overall SMB is underestimated. These changes relate to the sensitivity of accumulation and melt to the resolution of topography. The GEOS-5 SMB fields contrast with available corresponding atmospheric models simulations from phase 5 of the Coupled Model Intercomparison Project (CMIP5). It is found that only a few of the CMIP5 AGCMs examined provide significant summertime runoff, a dominant feature of the GrIS seasonal cycle. This is a condition that will need to be remedied if potential contributions to future eustatic change from polar ice sheets are to be examined with GCMs.

1. Introduction

The Greenland Ice Sheet (GrIS) influences global climate in part through the storage and release of freshwater into the ocean. Changes in mass of the grounded ice sheet resulting in freshening of the adjacent ocean through runoff and discharge have implications for global sea level and for North Atlantic thermohaline circulation (e.g., Fichefet et al. 2003; Gerdes et al. 2006). In recent years, the GrIS has made a positive contribution to global sea level rise (e.g., Hanna et al. 2013; Bindoff et al. 2007; Shepherd et al. 2012). Vaughan et al. (2013) characterize as "very likely" that the rate of ice loss from the GrIS over the last two decades has accelerated, and that the loss is equally partitioned between outlet glacier discharge and surface melt (van den Broeke et al. 2009). Surface mass balance (SMB)—the balance of accumulation minus surface wastage terms—is thus an important variable for the evaluation of GrIS conditions. Along with surface temperature, SMB is a fundamental input

Corresponding author address: Richard Cullather, NASA/GSFC, Code 610.1, 8800 Greenbelt Road, Greenbelt, MD 20771.
E-mail: richard.cullather@nasa.gov

DOI: 10.1175/JCLI-D-13-00635.1

field for dynamical ice sheet models (ISMs) used in prognostic assessments of GrIS total ice volume and glacier discharge (Bindschadler et al. 2013; Nowicki et al. 2013; Alley and Joughin 2012). In the evaluation of ISMs, uncertainty associated with external surface forcings has been found to be as important as uncertainty produced by the different formulations of the models themselves (Nowicki et al. 2013).

Interest in examining the surface representation of the GrIS in general circulation models (GCMs) is motivated by a need to assess changes to its eustatic contribution under potential climate scenarios and to understand how the partitioning of the contribution might change with time (e.g., Parizek and Alley 2004). Skill in reproducing GrIS SMB is known to vary widely among GCMs. For example, Smith (1999) found that "realistic" estimates of SMB terms were obtainable from integrations with a 1⅞° grid interval (approximately 200 km × 70 km), while Murphy et al. (2002) and Bengtsson et al. (2011) found that simulated GrIS SMB became unrealistically negative for grid spacings of 125 km or greater. Two issues of relevance for GCM simulations are 1) the spatial resolution afforded by the model grid and 2) the extent to which physical processes are represented. With regards to spatial resolution, Meehl et al. (2007) observed that GCMs surveyed in the Fourth Assessment Report of the Intergovernmental Panel on Climate Change (IPCC AR4) were unable to produce a "good simulation" of SMB, in part because the available spatial resolution was insufficient to adequately resolve the coastal escarpment of ice sheets and its associated orographic effects on precipitation and melt (e.g., Glover 1999). In the Fifth Assessment Report (AR5), Flato et al. (2013) noted that agreement with observations is limited for the polar ice sheets. Church et al. (2013) further indicated that resolution of a few tens of kilometers or finer is necessary to resolve strong gradients in the SMB field. Efforts have been made to apply downscaling approaches for producing a higher-resolution SMB field from GCMs (Hanna et al. 2005; Agosta et al. 2013; Bougamont et al. 2005; Jarosch et al. 2012; Mernild and Liston 2012). These strategies are advantageous for coupling with ISMs, which have spatial resolutions of a few kilometers or less (Pollard 2010; Lipscomb et al. 2013; Ridley et al. 2005; Vizcaíno et al. 2010).

With regards to physical processes including surface albedo, snow ageing, and the treatment of melt, IPCC reports indicate deficiencies in the representation of these phenomena in GCMs. Deficiencies in SMB fields produced by AR4 models were found to be a result of limitations in the land surface schemes employed, which lacked a representation of meltwater refreezing within the snowpack and snow albedo variations (Meehl et al. 2007). In addition, the effects of GrIS meltwater runoff on the North Atlantic meridional overturning circulation were commonly not included in AR4 simulations (Randall et al. 2007). More recently, the AR5 report also noted that ice sheet processes were not generally well represented in climate models (Bindoff et al. 2013). Several recent studies have advanced more sophisticated surface schemes as an essential step for an improved SMB representation (Punge et al. 2012; Vizcaíno et al. 2013). As surface processes on the GrIS have characteristic length scales and occur in particular regions (Wild et al. 2003; Quiquet et al. 2012), spatial resolution and model complexity are significantly linked. This needs to be taken into consideration for an evaluation of the ice sheet surface representation.

In this study, an improved surface representation is evaluated in atmospheric GCM (AGCM) integrations of the contemporary climate at both coarse and high spatial resolution. The Goddard Earth Observing System model, version 5 (GEOS-5) is assessed in comparison to a standard model configuration, available observational datasets, and other GCMs. The paper is organized as follows. Section 2 describes the GEOS-5 model and the implementation of Stieglitz snow hydrology model over glacial surfaces. Datasets used for assessing model performance are also described. An appraisal of the effects of the snow model on the general climate in comparison to the control simulation are provided in section 3, as well as a detailed assessment of the resulting surface energy balance and SMB. A discussion of the results is given in section 4.

2. Model description, datasets, and method

GEOS-5 is an AGCM maintained by the National Aeronautics and Space Administration Global Modeling and Assimilation Office (NASA GMAO; Rienecker et al. 2008; Molod et al. 2012). The GEOS-5 AGCM is used for decadal climate prediction studies and as the atmospheric component in coupled model simulations (Ham et al. 2012a,b), as well as for routine numerical weather prediction (Reale et al. 2009), and serves as the background atmospheric model in the data assimilation system used for the Modern-Era Retrospective Analysis for Research and Applications (MERRA; Rienecker et al. 2011). The model employs a finite-volume dynamical core (Lin 2004) that is integrated with various physics packages. In the version of GEOS-5 used for this study, a 30-arc-second version of the global elevation dataset of the Shuttle Radar Topography Mission (SRTM30; Farr et al. 2007) is supplemented by data over polar ice sheets (Bamber et al. 2001; Liu et al. 2001).

The GEOS-5 land surface model is catchment-based, wherein a topographical index denotes a set of tiles

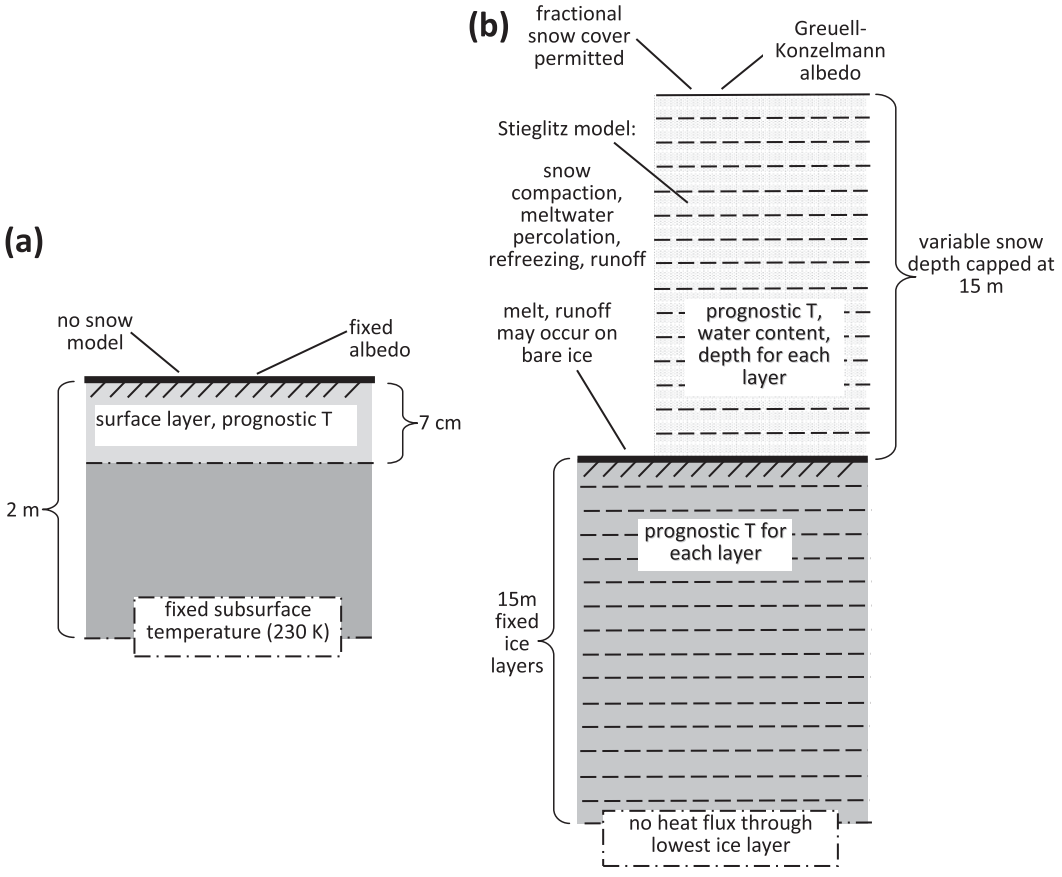

FIG. 1. Schematic indicating the representation glaciated ice surfaces in the GEOS-5 model: (a) in the original state and as represented in MERRA reanalysis, and (b) with application of snow model and ice representation.

occupying fractional areas below each atmospheric grid column (Koster et al. 2000). These tiles are used to indicate land surface types that represent subgrid-scale heterogeneity in prognostic hydrologic variables, such as soil moisture. The index of each subgrid-scale catchment tile is determined from a high-resolution raster—currently from the 5-km resolution dataset of the U.S. Geological Survey (USGS) Global Land Cover Characterization project (Loveland et al. 2000). Fluxes computed on surface tiles are related to the atmospheric column via an exchange grid.

The terrestrial (i.e., nonglacial) land surface model in GEOS-5 employs a modified version of the Stieglitz snow hydrology model, which provides an explicit representation of snow densification, meltwater runoff, percolation, refreezing, and surface albedo (Lynch-Stieglitz 1994; Stieglitz et al. 2001). In the adaptation for GEOS-5, the Stieglitz model has three layers when snow cover is present, with a maximum thickness of the top layer not exceeding 8 cm. For each layer, prognostic variables of heat content, equivalent snow water content, and snow depth are maintained. A volumetric water holding capacity is denoted for each layer. Snow compaction is based on the parameterization of Kojima (1967). A maximum snow density of 500 kg m^{-3} is prescribed, with snow mass exceeding this value becoming runoff. The snow model includes representations of processes including snowpack growth and ablation, melting, refreezing, and sublimation. For GEOS-5, snow albedo is prescribed based on a linear relation with snow density in the uppermost layer, with reductions imposed by vegetation masking and fractional snow cover. For a given model time step, the land surface scheme solves for the energy balance at both the snow–atmosphere and the land–snow interfaces.

On grounded ice, hydrologic processes including runoff were not considered in the original model configuration; hence, an ice-sheet SMB was not produced. Ice sheets were represented as a 7-cm water-equivalent (w.e.) surface ice layer (Fig. 1). The temperature corresponding to this surface ice layer was determined from turbulent, radiative, and subsurface energy fluxes using semi-implicit time stepping. In the original model configuration, the subsurface energy flux was determined

from the prognostic surface layer temperature and a fixed temperature of 230 K at 2-m depth, and the land–ice surface albedo was fixed at 0.775. These values were applied in early model development, but are thought to have been selected as representative of the climate of polar ice sheets. In the semi-implicit scheme, atmosphere and ice surface temperatures respond mutually to these parameterizations. Cullather and Bosilovich (2012) examined the surface energy budget in MERRA over Greenland and Antarctica. The subsurface energy parameterization was found to produce spurious annual mean flux imbalances of up to 30 W m^{-2} locally. The motivation for addressing limitations in the surface representation over grounded ice in GEOS-5 thus included the need to remedy existing limitations in the surface energy budget representation as well as to produce a realistic estimate of runoff for use in a coupled atmosphere–ocean–dynamical ice sheet model configuration.

Over glaciated surfaces, snowfall typically exceeds summer melt. Snow hydrology representations commonly used in GCMs over nonglaciated surfaces accumulate snow without a mechanism for converting it to glacial ice and, over time, would produce a snowpack over ice sheets with nonphysical depth. While this does not constitute a direct impediment to the performance of the atmospheric model, the conducted heat flux and other properties may not be adequately parameterized or resolved with available resources through an unrealistically deep snowpack, thus having an adverse effect on simulated surface energy fluxes. To compensate, the use of a snow hydrology model over ice sheets is often prohibited as in the original version of GEOS-5, or a cap on the size of the snowpack is provided (e.g., Lipscomb et al. 2013). Snow mass exceeding the cap in snow depth or in density is then directly routed to the oceans. This excess term is often referred to as ''frozen runoff'' and may be seen as a poor man's simulation of ice calving. The criteria necessary for an improved land ice surface representation may then be seen as maintaining consistency with the snow hydrology representation used on other terrestrial surfaces while accommodating specific issues associated with snowfall on ice sheets.

The new configuration for land ice surfaces (Fig. 1b) indicates an implementation of the snow hydrology model with a cap on the maximum snow depth at 15 m. This depth is comparable with other models (e.g., Bugnion and Stone 2002). In practice, snow depth is limited by the Stieglitz model maximum value for snow density and is typically less than half the imposed maximum depth at any location. In this elemental approach, the Stieglitz model operates as it does over nonglaciated surfaces, but with an increased vertical resolution of 15 layers to adequately simulate the heat flux through the snowpack. The upper five layers of the snowpack are constrained in depth to resolve the near-surface temperature gradient, with the topmost snow layer restricted to a maximum thickness of 8 cm. Snow cover over ice is allowed to be fractional, and melting and runoff may occur on exposed bare ice surfaces. A 15-layer ice column is applied for the conduction of heat below the snow–ice interface, with a zero heat flux condition imposed at the lower boundary. Surface radiative properties for the snowpack are taken from Greuell and Konzelmann (1994), in which albedo is a linear function of snow density in the uppermost snow layer. In this relation, albedo decreases more rapidly with increasing snow density than is prescribed by Stieglitz et al. (2001). This is to account for the higher density of fresh snow found over ice sheets (Greuell and Konzelmann 1994). Recent studies have found more realistic representations of snow albedo using parameterizations of snow grain size rather than snow density as used in GEOS-5 (van Angelen et al. 2012). In particular, a density-dependent albedo scheme was found to underestimate albedo in wet snow conditions. Nevertheless, credible results are obtainable with snow density parameterizations (e.g., Ettema et al. 2009, 2010a,b; Slater et al. 1998). A value of 0.6 is used for bare ice albedo. Additional characteristics of the snow model are as previously described in Lynch-Stieglitz (1994) and Stieglitz et al. (2001). Thus for the new configuration, snow hydrology over land ice remains consistent with that used over nonglaciated surfaces, with the exception of increased vertical resolution for larger snow depths and modification of the snow albedo parameterization.

The approach of this study is to evaluate the performance of the GrIS surface representation in Atmospheric Model Intercomparison Project (AMIP)-style (Gates et al. 1999) simulations of GEOS-5 forced with sea ice and sea surface temperature (SST) fields for the period 1979–2008 (Reynolds et al. 2002). Two simulations are run at a horizontal resolution of 2° latitude by 2½° longitude and 72 hybrid-sigma coordinate vertical levels. Two simulations of ½° × ⅝° are also presented and will be the main focus for comparisons with in situ observations. Hereafter, these simulations are referred to as GSN2 for the 2° integrations using the snow hydrology model over land ice regions, GSN½ for the ½° run using the snow hydrology model, and CNTRL2 and CNTRL½ for the control simulations at 2° and ½°, respectively. Figure 2 shows the differences in the spatial representation of Greenland topography. While model GrIS elevations are both initially based on Bamber et al. (2001), the process leading to model topography that is appropriately scaled for each GCM spatial resolution is complex. The ½° model topography closely

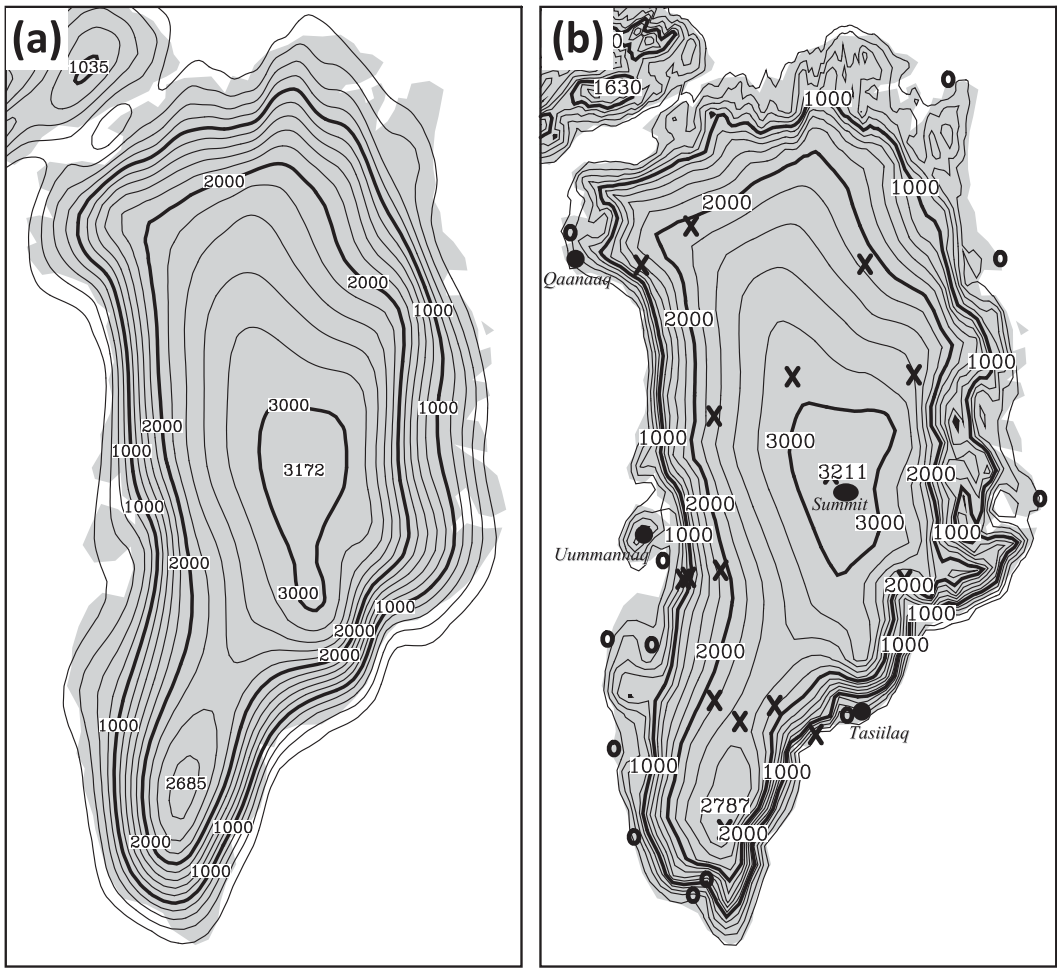

FIG. 2. Greenland topography used for (a) 2.0° × 2.5° and (b) 1/2° × 5/8° grid spacing. The contour interval is every 200 m, with heavier line and labels for every 1000-m contour . In (b), AWS are indicated with an "X" for GC-Net stations and "O" for DMI stations. Place names used in text are labeled.

approximates that of Bamber et al. (2001). The 2° model topography is lower over the central and western areas of the GrIS, but the 200-m contour encompasses a larger area. Surface characteristics in these simulations are compared with the control simulation, with contemporary GCM and regional model output, and with available observations and gridded datasets. These include available in situ observations of surface temperature, energy fluxes, and glaciologically derived SMB, and with gridded fields of satellite-derived temperature and prognostic SMB from regional climate models and from the Interim European Centre for Medium-Range Weather Forecasts (ECMWF) Re-Analysis (ERA-Interim, herein ERA-I; Dee et al. 2011). Monthly fields of ERA-I were obtained for the years 1980–2008 at a regular grid spacing of 0.75° × 0.75°. A collection of 15 automatic weather stations (AWS) known as GC-Net are distributed on the GrIS and report hourly measurements of temperature, wind, surface radiation fluxes, and other variables (Steffen and Box 2001). Twelve AWS stations from the Danish Meteorological Institute (DMI; Carstensen and Jørgensen 2011) located on nonglaciated land surfaces on the GrIS periphery are also used. Additional datasets are described in context below.

3. Results

a. Surface energy budget

From the perspective of the atmospheric model, the net surface energy flux is the sum of radiative flux components and turbulent fluxes of sensible and latent heat. In the absence of melt processes, it is in agreement with the ground flux through the ice. For the control model version of GEOS-5, the annual mean simulated net surface energy flux over the GrIS consists of a large downward (negative) flux of greater than 25 W m^{-2} in

coastal regions and greater than 5 W m^{-2} over the ice sheet interior. This result from AMIP simulations is similar to MERRA (Cullather and Bosilovich 2012). The flux results from the fixed subsurface temperature parameterization of 230 K. While the parameterization was thought to provide a more realistic diurnal cycle, the annual mean surface flux magnitudes are erroneous. Net surface energy fluxes over ice sheets may result from geothermal sources but are thought to be small (e.g., Reijmer and Oerlemans 2002) and are not explicitly simulated here. The annual net surface flux may also differ from zero in locations of surface melt or refreezing. For the new scheme depicted in Fig. 1b, the net surface flux is near zero for the bulk of the GrIS with the exception of small coastal regions. In particular, magnitudes greater than (−) 10 W m^{-2} are found only on the southwestern edge of the GrIS, associated with surface melt. For the new scheme, a net heat flux of zero is not guaranteed over nonmelting land ice surfaces because of the removal of mass associated with capping the snow density and depth, but this heat flux due to ''frozen runoff'' is small.

Hoch (2005) obtained radiative flux values at Summit (73°N, 38°W) for the period July 2000 to July 2002, and turbulent flux values from a 50-m tower for the period June 2001 to July 2002. Components of the surface radiative flux were also obtained from AWS stations as part of the Programme for Monitoring of the Greenland Ice Sheet (PROMICE) for the period 2008–10 (van As and Fausto 2011), and as part of the Greenland Analog Project along the Kangerlussuaq transect (K-transect) on the western GrIS near 67°N for the period 2003–10 (van den Broeke et al. 2008). K-transect site 9 (S9) was located within 91 km of the western ice margin. The PROMICE AWS stations are also typically located along the periphery of the GrIS.

Comparisons of the ½° model with Summit observations shown in Fig. 3a indicate disagreements with the surface net flux from the CNTRL½ simulation of greater than 20 W m^{-2} in summer months, and an annual mean difference of 8 W m^{-2}. This summertime bias in the net flux is eliminated with the new surface representation. The improvement results from a better treatment of the shortwave flux, and error cancellation. As seen in Fig. 3b, differences with the July observed net shortwave flux are reduced, from 20 W m^{-2} for the CNTRL½ simulation to 11 W m^{-2} in the GSN½ run. An important component of the improved representation is the Greuell and Konzelmann (1994) surface albedo parameterization. The application of the surface model allows the surface albedo to develop spatial heterogeneity, as shown in Fig. 4 for July. A considerable area of the ice sheet above the ablation zone has simulated albedos greater than the 0.775 prescribed value in the control simulation. The spatial distribution shown in Fig. 4 is comparable to that given by Vizcaíno et al. (2013) for the Royal Netherlands Meteorological Institute's (KNMI's) Regional Atmospheric Model version 2 (RACMO2) and the Community Earth System Model (CESM). In contrast to improvements found in the shortwave flux representation, an underestimate of the annual mean net longwave flux of 12 W m^{-2} is increased in the GSN½ run to 16 W m^{-2}. The turbulent flux values from GSN½ are not significantly different from the control.

For K-transect station S9 (Fig. 3c) located within the ablation and percolation zone, a net surface flux bias of 18 W m^{-2} in CNTRL½ winter is reduced to 2 W m^{-2} in the GSN½ run. As with Summit, there is better agreement between the observed and new model simulated net shortwave flux in summer and autumn as compared to the control (Fig. 3d). But improvement in the net flux in winter largely results from changes in turbulent fluxes as compared with the control simulation. A sensible heat flux bias of 32 W m^{-2} in January in the control model is reduced to 20 W m^{-2} for the GSN½ model. However, differences between model and observation for the net longwave flux are again larger with the new surface parameterization. The annual mean bias in the net longwave flux is 2 W m^{-2} for CNTRL½ but 15 W m^{-2} for GSN½. Comparisons with other K-transect and PROMICE AWS locations indicate similar biases in the net longwave flux. In comparison to four PROMICE stations located on the GrIS, there is an underestimate of the modeled annual net longwave flux for the GSN½ model of 3 to 9 W m^{-2}. These biases are found to result from an underestimate of the downwelling component. For the GSN½ simulation, surface temperatures are improved in comparison to the CNTRL½ model such that a compensating bias in the upwelling longwave flux is reduced, and an underestimate in the downwelling flux remains. This is related to the underestimation of clouds, atmospheric humidity, and/or transmissivity, and is common to most atmospheric models.

Figure 5 presents a comparison of averaged near-surface air temperatures from GC-Net and DMI stations with model values from the ½° simulations. For winter months, temperatures from the CNTRL½ and GSN½ simulations compare similarly, and the skill is comparable to other climate models (e.g., Rae et al. 2011). In both simulations, near-surface December–February (DJF) air temperatures correlate well with GC-Net (r = 0.98) and coastal DMI stations (r = 0.96). The model is biased by −2.6°C in comparison to GC-Net and +1.1°C in comparison to DMI.

Important differences occur between the two simulations in summer months. For the interior GC-Net

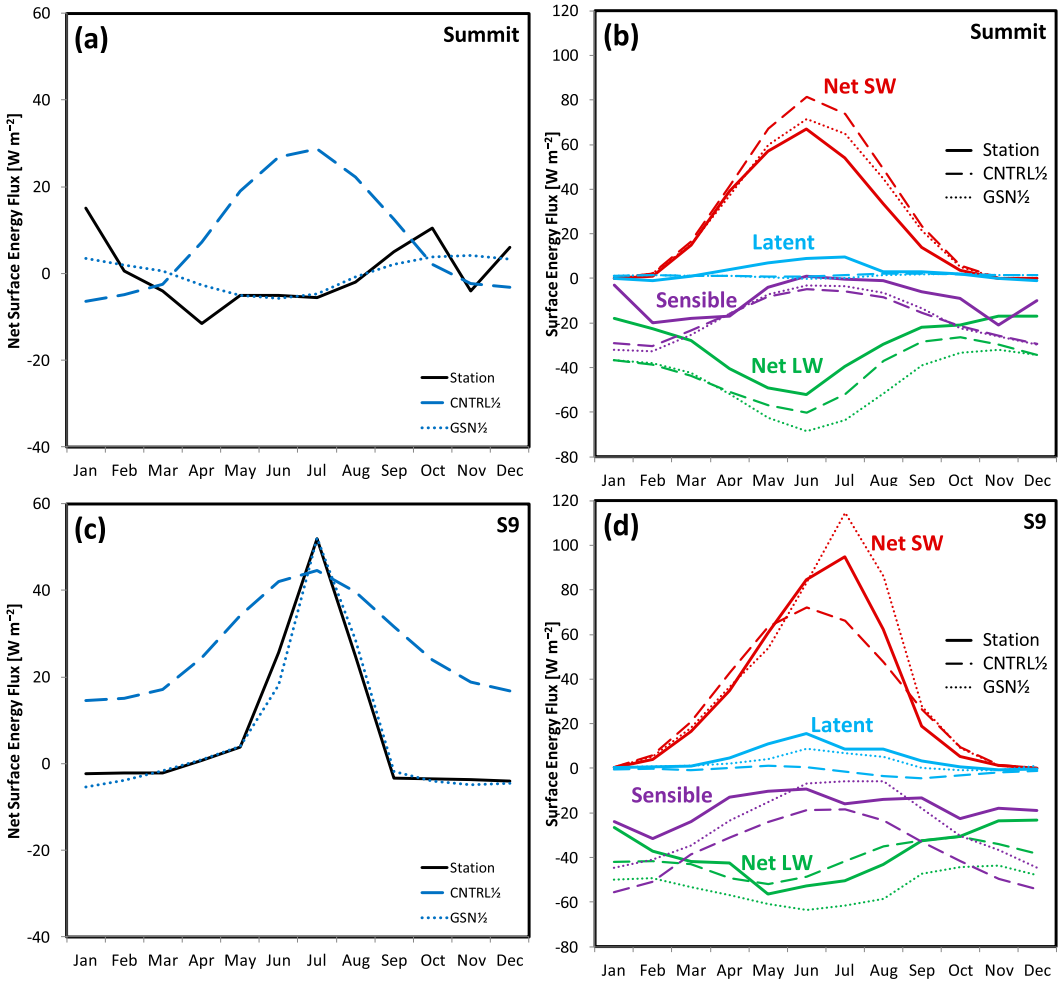

FIG. 3. The (a) net surface energy flux and (b) surface radiation (positive downward) and turbulent heat flux components (positive upward) from GEOS-5 ½° AMIP simulations in comparison to 2000–02 observations at Summit (72°35′N, 38°30′W; Hoch 2005), and the corresponding (c) net flux and (d) surface radiation and turbulent heat flux components for the S9 station within the ablation and percolation zone along the K-transect (67°3′N, 48°14′W; van den Broeke et al. 2008). Model fluxes are averaged for the period 1980–2008. Bold solid lines indicate observed station values, dashed lines correspond to the CNTRL½ integration, and dotted lines indicate the GSN½ simulation (in W m^{-2}).

stations, the average June–August (JJA) temperature bias is −4.4°C for the CNTRL½ simulation, but −1.4°C for the GSN½ run. Larger differences between the simulations occur for locations with warmer observed temperatures. For locations warmer than −5°C, the GSN½ simulation is 3.8°C warmer than the control. For locations observed colder than −10°C, the new scheme is 2.8°C warmer. This implicates the use of a cold, fixed subsurface temperature in the control simulation. The correlation between summer observed and simulated values is also slightly improved with the new parameterization, from $r = 0.96$ for the control to $r = 0.97$ for the new parameterization. For DMI stations, the average bias is reduced from −2.6°C in the control to −1.7°C with the new scheme, and the correlation has increased from $r = 0.80$ to $r = 0.84$.

The spatial agreement may be further evaluated using monthly temperature data derived from the Moderate Resolution Imaging Spectroradiometer (MODIS; Hall et al. 2012), which were obtained for the period 2003–10. For comparison with MODIS, the model temperature was computed from the clear-sky emitted longwave flux field from the surface. The difference between the summertime model-computed temperature and MODIS for the CNTRL½ simulation is shown in Fig. 6a. The figure shows magnitudes greater than (−) 2°C over most of the GrIS, with largest differences of greater than (−) 4°C inland from the southeastern escarpment and greater

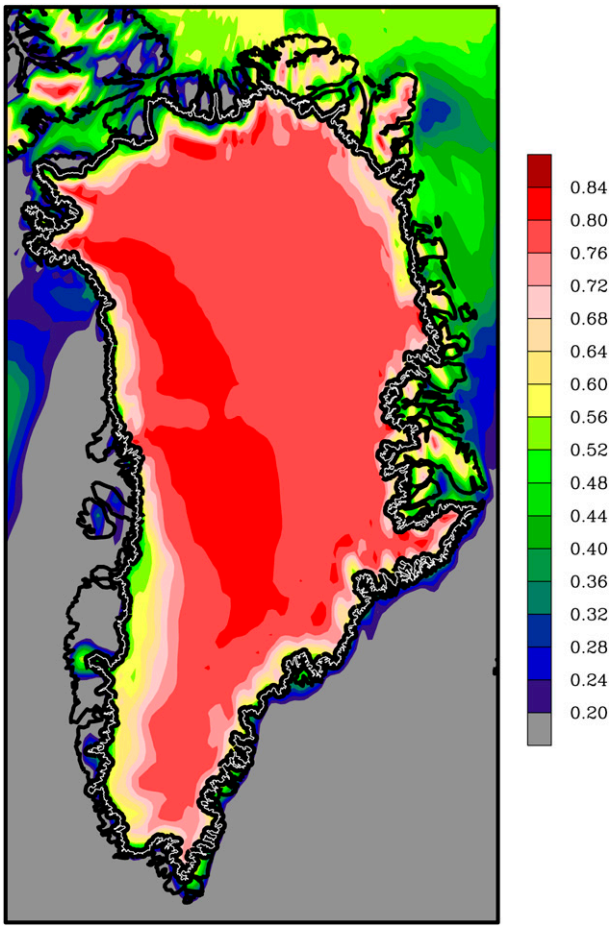

FIG. 4. The 1980–2008 averaged July surface albedo from the GEOS-5 GSN½ simulation. The contour interval is 0.04. The margin of the ice sheet (Zwally et al. 2012) is indicated with a white line.

than (−) 5°C adjacent to the Scoresby Sund. Some edge effects are also apparent, particularly in the northern regions. With the new surface representation shown in Fig. 6b, these differences are greatly reduced over much of the GrIS, with values colder than MODIS by more than 2°C in the southeast, and more than 3°C warmer along the western edge of the ice sheet. MODIS ice surface data are known to have a cold bias in comparison with thermochron-derived surface temperatures (e.g., Hall et al. 2012; Koenig and Hall 2010). Nevertheless, the comparison shown in Fig. 6 indicates a substantial correction to surface temperatures with the new surface scheme.

The evaluation of subsurface conditions is even more challenging, owing to a lack of reliable contemporary observational data. Observations from the GC-Net AWS network include subsurface temperature profiles produced from a thermocouple string. Such measurements are problematic, as the vertical position of the string may change with time in an unknown manner from accumulation or settling (Steffen and Box 2001). Nevertheless, a comparison of the modeled annual temperature wave with observations at two representative stations (Fig. 7) shows similarities with the observed rapid damping with depth. For a low accumulation site, the simulated 10-m-depth annual cycle magnitude at TUNU-N (78°01′N, 33°59′W) of 0.7°C in GSN½ is comparable with the observed value of 0.5°C. This location may be contrasted with Swiss Camp (69°34′N, 49°20′W), where interannual variability is large (Steffen and Box 2001).

Here the 10-m depth annual temperature wave magnitude in GSN½ of 1.2°C compares with 0.7°C from observations, and there is a bias of 2.5°C in the mean annual temperature. As well as measurement uncertainties, differences in the simulated magnitude of the annual cycle in the upper 3 to 4 m may also result from comparison of point observations with the AGCM grid box. Given the uncertainties, such differences are not unexpected (e.g., Bugnion and Stone 2002).

The differences in the surface energy budget resulting from the new surface representation affect the local and regional atmospheric circulation. Shown in Fig. 8a are the pan-Arctic temperature differences between the CNTRL½ and GSN½ simulations for summer months. Note that again the largest temperature differences on glaciated land surfaces occur in locations where the surface values differ significantly from the 230-K parameterized ice value of the control simulation. These locations are along the periphery of the GrIS. Smaller glaciated surfaces are apparent, including Ellesmere, Svalbard, and the Juneau Icefield. The difference in the pan-Arctic sea level pressure field shown in Fig. 8b indicates a local deepening of the pressure field in the North Atlantic near Greenland of about 1.5 hPa. The differences of the two model simulations are significant but are less than the observed interannual variability at coastal stations in southeastern Greenland. For example, the standard deviation of the observed JJA sea level pressure at Tasiilaq (65.6°N, 37.6°W) is 2.3 hPa for the period 1980–2008. The pressure differences reflect a dynamical response to warming of the ice sheet periphery. These differences also appear to influence the wave-2 pattern of the Northern Hemisphere, with a significant lowering of the pressure field over Siberia.

b. *Surface mass balance*

The ice-sheet SMB may be approximated by the net of three terms: precipitation—the vertical flux of solid and liquid water phases between the atmosphere and the surface; evaporation—the net vertical flux of water vapor between the surface and the atmosphere; and runoff—the net horizontal divergence of liquid water

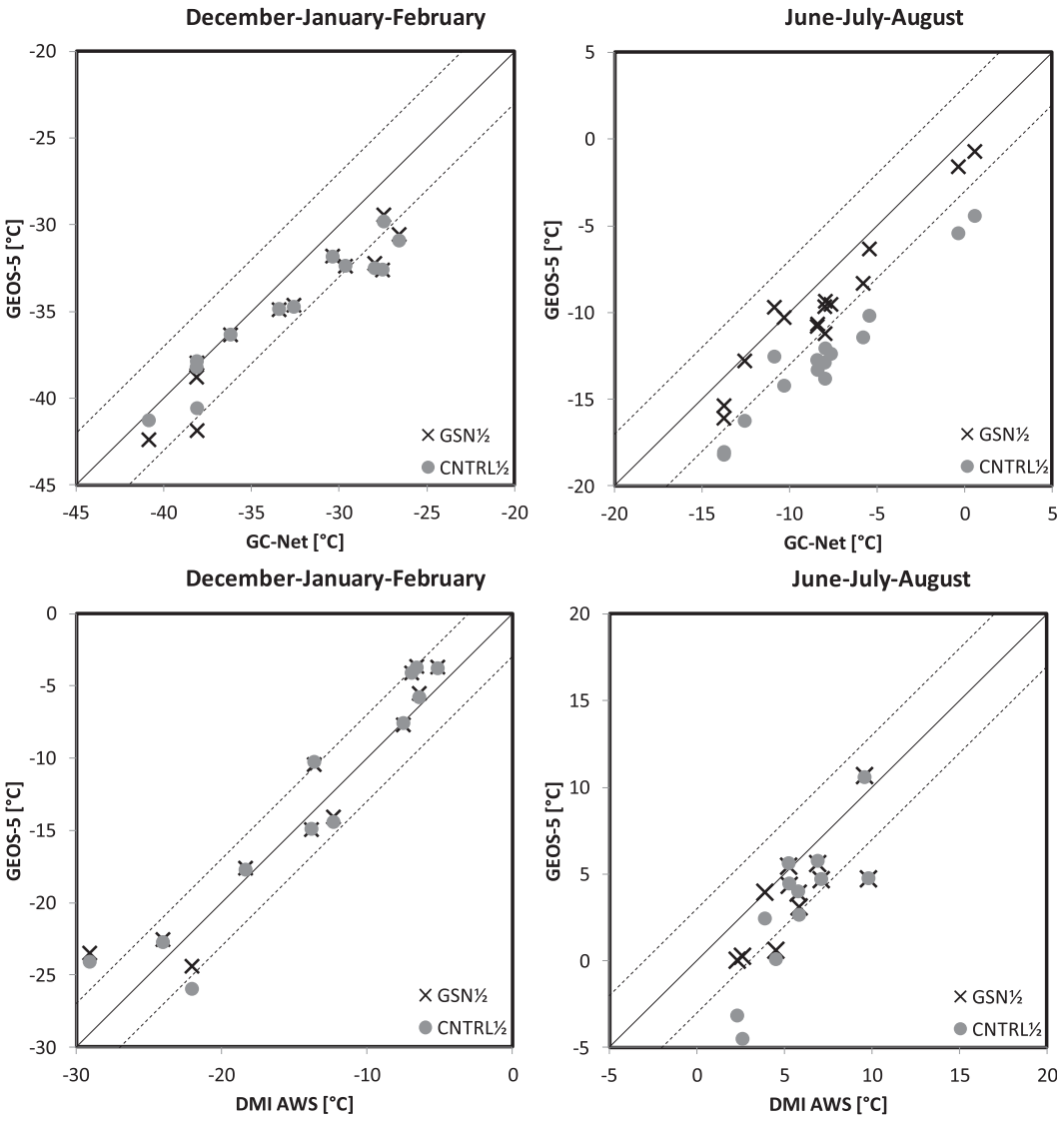

FIG. 5. Comparison of average Greenland AWS near-surface air temperatures from (top) 15 interior GC-Net locations and (bottom) 12 coastal DMI stations with corresponding CNTRL½ and GSN½ simulated values, in °C. Station locations are indicated in Fig. 2. Model temperatures are taken from the nearest grid point and corrected to station elevation using the dry-adiabatic lapse rate. Diagonal lines denote exact correlation and ±3°C.

at the surface. Other terms including blowing snow are considered negligible here (e.g., Loewe 1970) although studies have estimated substantial values in winter for the GrIS (e.g., Lenaerts et al. 2012) and Antarctica (e.g., Budd et al. 1966).

Figure 9 shows the averaged annual SMB from GEOS-5 using the new surface representation at two different spatial resolutions. Again, the control version of GEOS-5 does not produce SMB. In the land surface scheme used in GEOS-5, surface characteristics for each fractional land surface type are aggregated to form a flux for the atmospheric model. For comparison with other models, the GEOS-5 fields shown in Fig. 9 are produced from the assembled global field, which includes non-glaciated land surfaces (runoff over oceans is zero).

Also shown for comparison are the regional climate model simulation of RACMO2 11-km integration (Ettema et al. 2009) interpolated to 5-km grid spacing (Bindschadler et al. 2013), and the average of accumulated 12-h prognostic integrations from ERA-I. The ERA-I surface fluxes denote the average of short-term model output initialized with assimilated observations, and have been shown to better agree with in situ observations than other analyses (e.g., Chen et al. 2011). The ECMWF model represents snow cover as one layer with a maximum depth of 7 cm, and meltwater percolation and

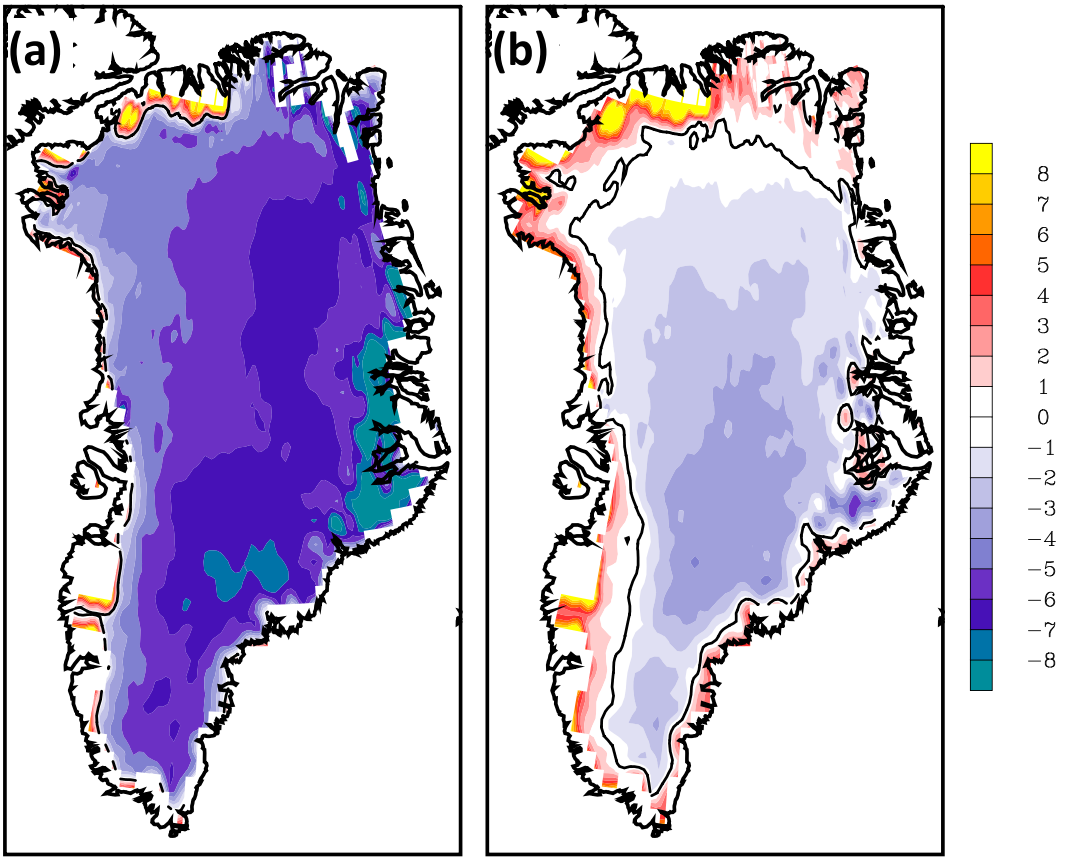

FIG. 6. Average JJA clear-sky surface radiance temperature from GEOS-5 1/2° AMIP simulations minus MODIS temperature values for (a) CNTRL1/2 and (b) GSN1/2 for 2000–08, in °C.

refreezing processes are not represented (ECMWF 2007; Ettema et al. 2010b). The ERA-I prognostic snow albedo follows the parameterization of Douville et al. (1995) and is a function of snow age (ECMWF 2007). ERA-I analyses are also used as lateral boundary conditions for the RACMO2 regional model. RACMO2 simulations are considered a state-of-the-art representation of SMB due to the use of high spatial resolution and representation of physical processes, and have been evaluated against in situ and satellite observations (e.g., Hanna et al. 2011; Shepherd et al. 2012). Results from the Modèle Atmosphérique Régional (MAR; Franco et al. 2012) are also cited. Church et al. (2013) characterized regional climate models as "the primary source" of ice-sheet SMB projections. The ERA-I SMB shown in Fig. 9 at 0.7° grid spacing presents the basic large-scale features for the GrIS as they are known, but with differences in the distribution of ablation zones as compared to RACMO2. Along the western escarpment of the GrIS, local maxima near Qaanaaq and the Uummannaq Fjord system seen in the RACMO2 field are not present in the ERA-I. The topographies of the given models and reanalyses are also indicated in Fig. 9. For RACMO2, the Bamber et al. (2001) topography is contoured.

The GSN1/2 simulation closely approximates the RACMO2 field in showing largest values of greater than 200 cm yr^{-1} w.e. in localized areas along the southeastern GrIS periphery and small values of less than 15 cm yr^{-1} w.e. (units equivalent to g cm^{-2} yr^{-1}) to the northeast and over the ice sheet plateau. The 1/2° simulation also reflects the location of the equilibrium line along the southwestern side of the GrIS, local maxima northeast of the Uummannaq Fjord system and near Qaanaaq (Thule), and the sharply defined ridge separating these two maxima. Areas of ablation along the north and northeastern periphery are also represented, and both models indicate values less than 30 cm yr^{-1} w.e. in a region extending southward from the plateau to near Tasiilaq. The GSN2 simulations indicate the large-scale features of GrIS SMB similar to RACMO2 and ERA-I, including large values in the southeast, smaller values over the northeast plateau, and enhanced values inland of the ablation zone along the western side of the ice sheet. However, the ablation areas along the western

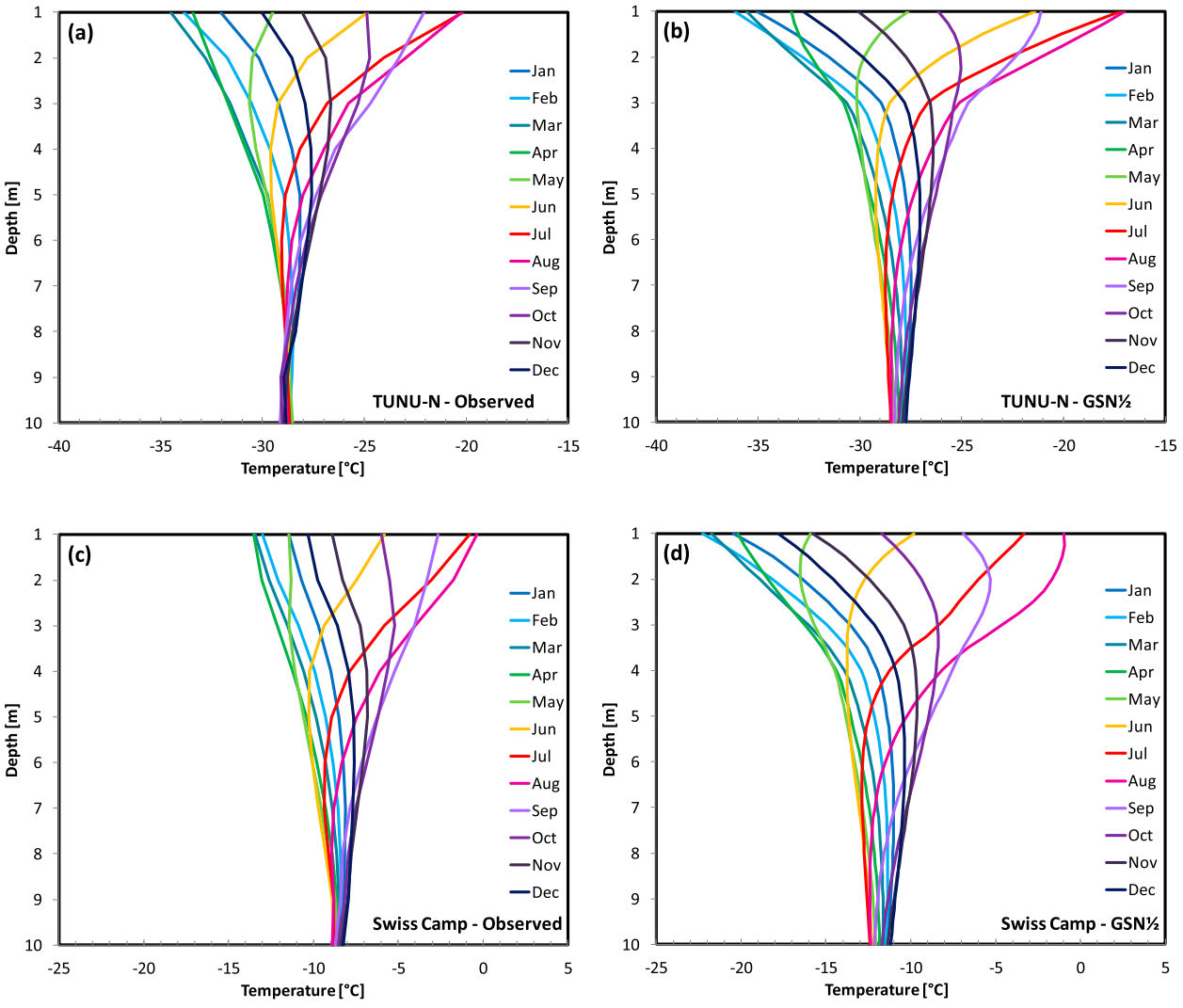

FIG. 7. The subsurface seasonal temperature cycle from (a) GC-Net AWS thermocouple temperature string at TUNU-N (78°01′N, 33°59′W), (b) simulation values for TUNU-N from GSN½, (c) GC-Net AWS values at Swiss Camp (69°34′N, 49°20′W), and (d) simulation values for Swiss Camp from GSN½, in °C. Values are averaged for the period 1996–2008.

and northern sides of the ice sheet are larger than in either RACMO2 or ERA-I, and more detailed features are largely absent. The effect of spatial resolution on the SMB distribution varies with location (Fig. 10). The southeastern maximum in SMB extends much farther into the interior of the ice sheet for the GSN2 field than for the higher-resolution GSN½ simulation. On the western side of the GrIS, the ablation zone is more narrowly defined and has greater magnitude at the higher spatial resolution, and there are larger values above the ablation zone.

Averages computed over the GrIS as defined by the 1.72×10^6 km^2 mask of Zwally et al. (2012) are shown in Table 1. The area encompasses GEOS-5 grid boxes of fractional land ice coverage along the GrIS periphery. For a particular GCM box along the margin, the fractional amount of area specified as land ice is dependent on the GCM grid spacing. Values obtained from only glaciated land surface tiles are indicated as "ice only." The total value includes tiles within a GCM box that are not glaciated, and is used for direct comparison with other models having unknown fractional ice sheet coverage within a grid box. It may be seen that the average for the GSN½ simulation of 26.7 cm yr^{-1} w.e. compares favorably to the RACMO2 estimate (27.4 cm yr^{-1} w.e.), while the 2° simulation value of 23.3 cm yr^{-1} w.e. is 15% less. For both model resolutions, the SMB computed using ice-only land surface tiles is smaller than the values computed from AGCM grid values. The ice-only values are 24.7 cm yr^{-1} w.e. for the GSN½ simulation and

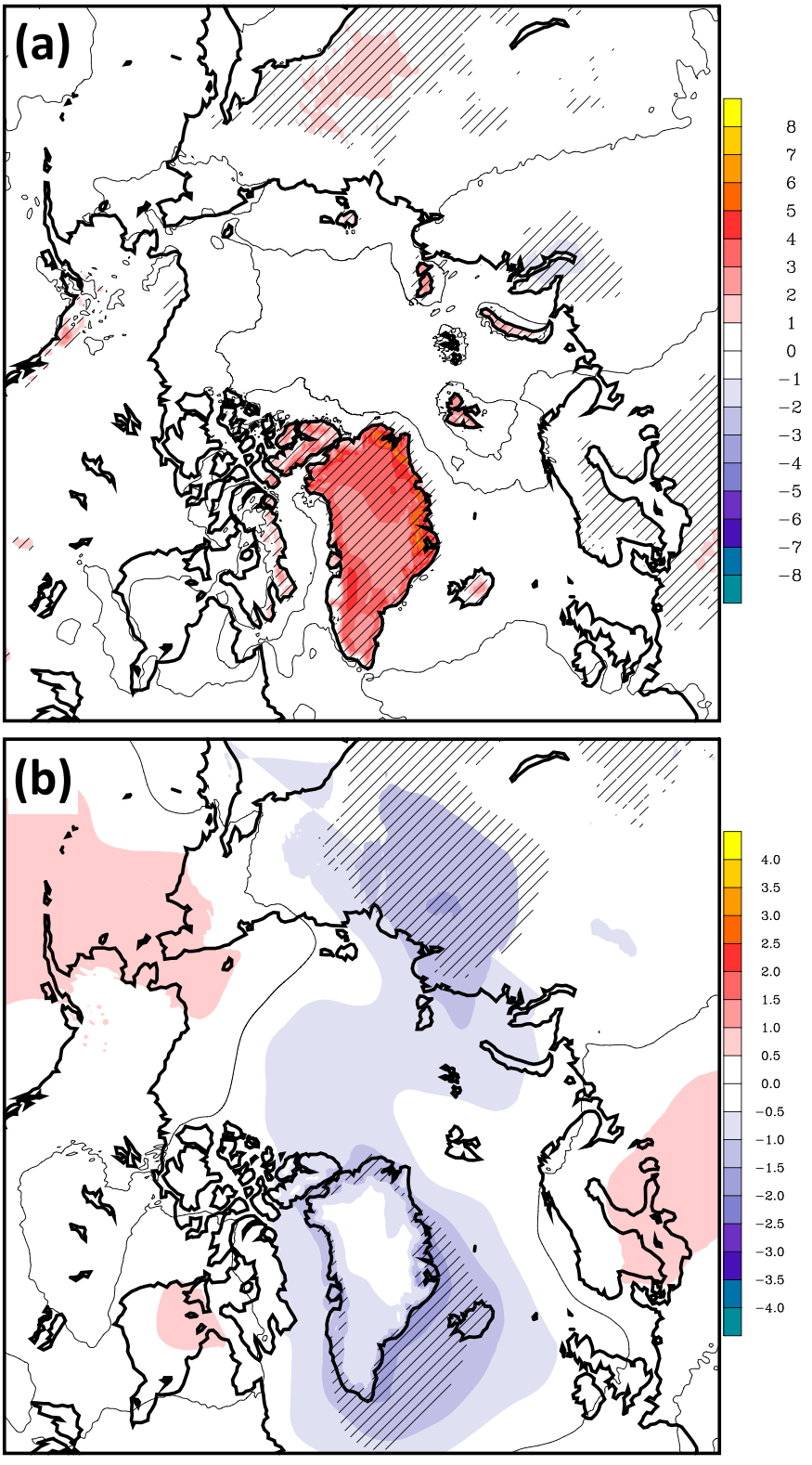

FIG. 8. Pan-Arctic difference of GSN1/2 AMIP simulation minus CNTRL1/2 for JJA (a) 2-m air temperature (in °C) and (b) sea level pressure (in hPa). Hatched areas indicate significance from the Student's *t* test at the 95% level.

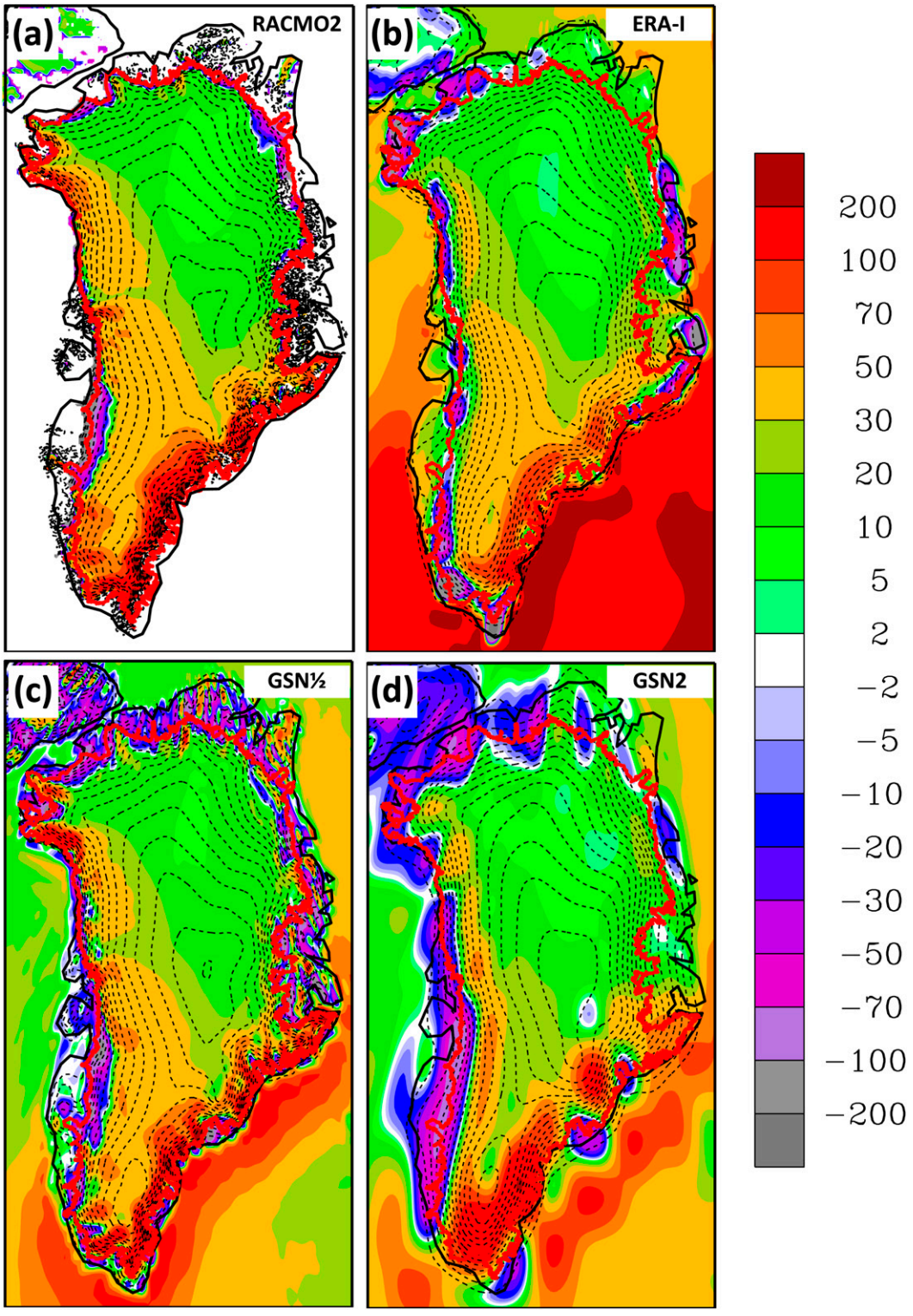

FIG. 9. Average surface mass balance from (a) RACMO2 for the period 1958–2007, (b) ERA-I for the period 1980–2008, (c) GSN$^{1}/_{2}$ simulation for 1980–2008, and (d) GSN2 simulations for 1980–2008 (in cm yr^{-1} w.e.). The ice sheet margin is indicated with a red line. Topography is indicated with dashed contours for every 200 m.

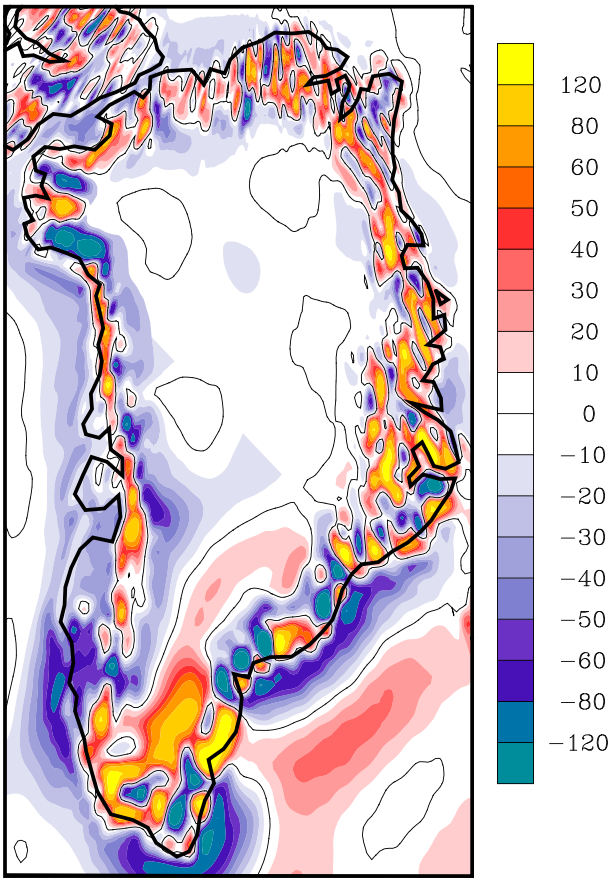

FIG. 10. The difference of GSN2 minus GSN½ average surface mass balance for 1980–2008 (in cm yr^{-1} w.e.).

18.2 cm yr^{-1} w.e. for the GSN2 integration. This is due to the larger amounts of runoff in peripheral ice-only tiles, as compared with AGCM grid values in which the runoff is averaged over both glaciated and nonglaciated land surface tiles. Table 1 shows a broad range of values for SMB components from RACMO2, MAR, and ERA-I. For precipitation, the GEOS-5 simulations provide values of less than 40 cm yr^{-1} w.e., which compare more favorably to ERA-I and MAR than to RACMO2. The GEOS-5 integrations were averaged over the period 1980–2008, which is similar to the published averaging period for MAR and the same period as for ERA-I, whereas RACMO2 was averaged over a 52-yr period. The GEOS-5 simulations, the reanalysis, and the regional climate models are in rough agreement in finding that evaporation has a small effect on the SMB. Interestingly, the GSN2 integrations find net deposition over the ice-only land surface tiles. As the peripheral Greenland topography extends over a wider area at coarser resolution, the northern interior regions of the GrIS are marginally more insulated from synoptic activity, and conditions are more conducive to sublimation. Finally, there is considerable uncertainty in the runoff term. The GSN½ simulation value from the new surface scheme of 15.0 ± 2.8 cm yr^{-1} w.e. compares with estimates from RACMO2 (14.5 cm yr^{-1}), MAR (10.1 cm yr^{-1}), and ERA-I (17.7 cm yr^{-1} w.e.).

A further evaluation of the SMB resulting from the new surface scheme is a comparison with the historical record of glaciologically derived SMB estimates. An inventory of 331 published values has been compiled by Bales et al. (2001), Bales et al. (2009), Cogley (2004), and van de Wal et al. (2012). A regression of these observations with values obtained from GEOS-5 integrations from interpolation of neighboring grid cells is shown in Fig. 11. Bales et al. (2001) separately listed historical records for years up to 1981 and more recent values. With notable exceptions, there is good agreement between the model SMB and the observations. Not surprisingly, the GSN½ simulation compares more favorably at point locations than the GSN2 run. The overall correlation is $r = 0.563$ for the GSN2 integrations and $r = 0.648$ for the GSN½ simulation. For the 2° model, there is a bias of −3.6 cm yr^{-1} w.e. with the observations, as compared to near-zero bias for the ½° simulation. But there is also a positive difference with observation at larger simulated SMB values from the GSN2 model as seen in Fig. 11a. This is principally associated with the Bales et al. (2001) historical observations taken in the southern part of the ice sheet.

Neither model resolution captures the large negative values tabulated in van de Wal et al. (2012). The observations were taken along the annually visited K-transect over the period 1990–2010, at elevations ranging from 383 to 1850 m. At the lowest elevation site, SMB was consistently estimated to be less than −4 m yr^{-1}, while the modeled net ablation did not exceed 1 m yr^{-1} for any of the K-transect locations. In a comparison with the CESM, Vizcaíno et al. (2013) find similar differences in SMB with the K-transect. Vizcaíno et al. (2013) attribute these differences to the location of these stations—in a tundra-surrounded fjord unresolved by the model—and to their location within the "dark zone," an outcropping ice layer containing dust from an earlier period (Wientjes and Oerlemans 2010). Excluding the observations of van de Wal et al. (2012), the correlation with in situ measurements is $r = 0.671$ for the GSN2 integrations and $r = 0.782$ for the GSN½ model.

A comparison of the simulated SMB has been made with ensemble members from 10 similar AMIP models obtained from the fifth phase of the Coupled Model Intercomparison Project (CMIP5) for the period 1980–2008 (Taylor et al. 2012). Not all of the participating CMIP5 models provided necessary variables—notably runoff—for computing SMB from the AMIP simulations. For some of the models, Gaussian fields have been

TABLE 1. SMB components precipitation (P), evaporation (E), and runoff (R) for the GrIS as defined by Zwally et al. (2012) from AMIP simulations of GEOS-5 and 10 models of the CMIP5 project for the period 1980–2008, corresponding reanalysis values from ERA-I, and regional climate model output (in cm yr^{-1} w.e.). The standard deviation of ensemble-averaged annual values is indicated in parentheses. The fractional ice sheet area above 2000-m elevation from simulation topography and the fractional area of ablation are given in percent.

	Ensemble No./ grid spacing	Area above 2000 m (%)	P	E	R	SMB	Ablation area (%)
GEOS-5	1/½°	61.1					
GSN½ (total)			40.3(3.8)	0.8(0.2)	12.8(2.6)	26.7(4.4)	10.6
GSN½ (ice only)			39.8(3.7)	0.1(0.1)	15.0(2.8)	24.7(4.5)	9.6
GEOS-5	2/2°	59.1					
GSN2 (total)			34.5(2.5)	1.6(1.5)	9.8(1.2)	23.3(2.7)	11.0
GSN2 (ice only)			33.7(2.5)	−0.5(0.1)	16.0(1.9)	18.2(3.3)	12.1
RACMO2[a]	—/11 km	61.0	43.4	1.5	14.5	27.4(2.4)	13.8[b]
MAR[c]	—/15 km		35.7	0.2	10.1	25.3	
ERA-I	—/0.75°	58.0	36.6(3.4)	1.4(0.2)	17.7(2.7)	17.6(3.8)	7.9
BCC-CSM1.1	3/3.6°	20.9	54.0(2.8)	5.9(0.4)	3.0(0.2)	45.2(2.7)	0.0
CanAM4	4/3.6°	41.7	39.3(2.4)	2.1(0.2)	7.2(0.9)	30.0(1.8)	0.0
CNRM-CM5	1/1.875°	53.2	38.7(5.3)	2.4(0.2)	11.2(2.1)	25.0(4.6)	7.7
GFDL-HIRAM-C180	3/0.5°	56.6	43.7(2.6)	2.1(0.1)	0.4(0.0)	41.2(2.5)	0.0
GFDL-HIRAM-C360	2/0.25°	57.5	42.4(3.3)	2.0(0.1)	0.2(0.0)	40.2(3.2)	0.0
GISS-E2-R	6/2°	55.7	40.5(2.4)	11.7(0.4)	0.2(0.1)	28.7(2.1)	2.5
IPSL-CM5A-MR	3/1.3°	60.5	41.7(3.2)	3.0(0.2)	0.6(0.1)	38.1(3.1)	0.0
MPI-ESM-LR	3/2.5°	44.3	42.7(2.8)	0.2(0.1)	0.6(0.1)	41.9(2.7)	0.0
MRI-CGCM3	3/1.5°	53.9	52.2(3.8)	−0.3(0.2)	6.0(0.7)	46.5(3.7)	0.1
NorESM1-M	3/1.875°	45.4	52.1(2.8)	2.7(0.2)	1.7(0.3)	47.8(2.6)	0.0

[a] For 1957–2008, from Ettema et al. (2009).
[b] Computed from interpolated 5-km grid.
[c] For 1990–2010, from Franco et al. (2012).

interpolated to an appropriate regular grid. While the models shown here provide a runoff variable, it is unclear from available documentation whether or not snow hydrology is explicitly simulated over the ice sheet, or if runoff results from peripheral nonglaciated land surfaces. The average SMB from models shown in Fig. 12 and Table 1 present a range of spatial resolutions and model skill. (Expansions of model names in Tables 1 and 2 are given in the appendix.) The coarse spatial resolution models of the Beijing Climate Center (BCC_CSM1.1) and the Canadian Centre for Climate Modeling and Analysis (CanAM4) depict only primary accumulation features of a maximum value along the southeast GrIS and a minimum region to the north. The remaining models, excluding those of the Geophysical Fluid Dynamics Laboratory (GFDL), approximate the 2° resolution of the coarse GEOS-5 simulations. Despite similarities in resolution among some of the models, the topographies are disparate, and are strongly related to both average SMB over the GrIS and local differences. Model topographies with a smaller area above 2000 m (Table 1) such as the BCC-CSM1.1 have higher values for precipitation. None of the models with grid spacing larger than 1.3° capture the magnitude of local accumulation features suggested by RACMO2. Higher-resolution models from the GFDL present detailed patterns of coastal SMB, similar to the GSN½ simulation and RACMO2. In particular, the HIRAM-C360 SMB field indicates local maxima associated with topographic features along the western ice sheet margins. Both simulations indicate ablation regions in western coastal Greenland, but confined to the nonglaciated land surface. It may be seen from Fig. 12 and is quantified in Table 1 that the RACMO2 and ERA-I SMB fields are composed of ablation areas that are greater than 7% of the GrIS. Apart from the GEOS-5 models, only the model from the Centre National de Recherches Meteorologiques (CNRM CM5) indicates similar ablation areas on the ice sheet.

The SMB values for these AMIP model simulations, averaged for the GrIS (Table 1), range from 25.0 to 46.5 cm yr^{-1} w.e. A large part of this range is attributable to differences in the amount of annual precipitation among the models, which ranges from 38.7 to 54.0 cm yr^{-1} w.e. But only 3 of the 10 models examined indicate amounts of runoff greater than 5 cm yr^{-1} w.e. These are CanAM4, CNRM-CM5, and MRI-CGCM3. CNRM-CM5 utilizes a variation of the Douville et al. (1995) snow hydrology scheme over polar ice sheets, and attains values for

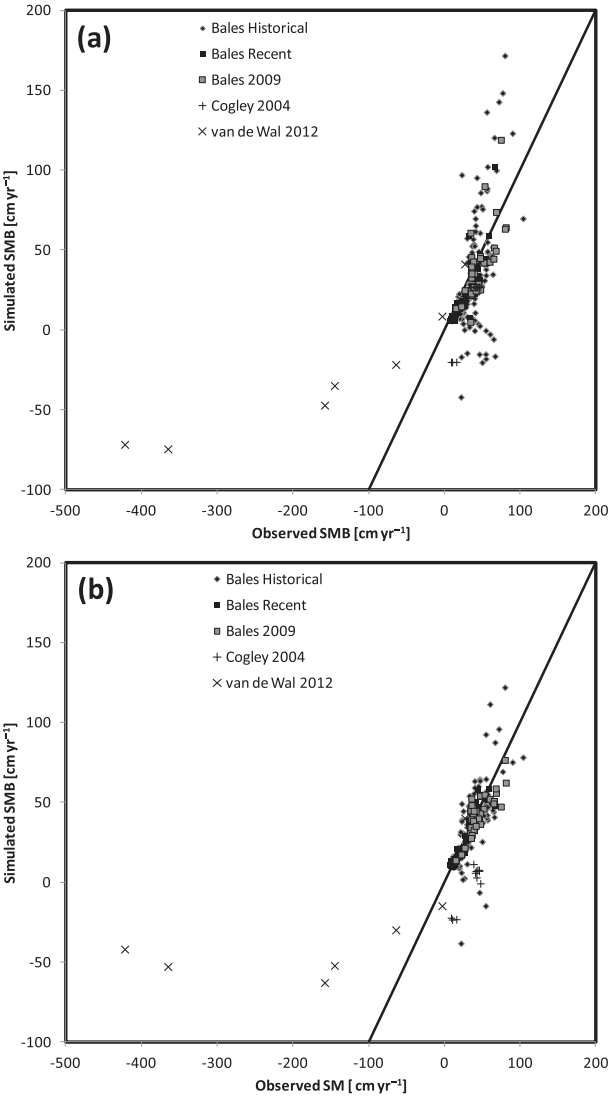

FIG. 11. Comparison of 1980–2008 average SMB interpolated from neighboring grid cells from (a) GSN2 and (b) GSN½ simulations of GEOS-5 with corresponding observations from historical and recent values from Bales et al. (2001), PARCA values from Bales et al. (2009), Cogley (2004), and van de Wal et al. (2012) (in cm yr^{-1} w.e.). See text. The diagonal line denotes a 1:1 comparison.

runoff and SMB comparable to RACMO2 and MAR regional models and the GEOS-5 simulations. Interestingly, the Goddard Institute for Space Studies (GISS) model (GISS-E2-R) provides a negligible amount of runoff over the GrIS but has the largest value among the AGCMs evaluated of 11.7 cm yr^{-1} w.e. for evaporation. In the averaged annual cycle of SMB (Fig. 13), summertime runoff is a dominant characteristic of the seasonal cycle of SMB in the reanalysis, and in the GEOS-5 models, with each indicating negative values over summer months. The results are similar to those presented by Vernon et al. (2013) using regional models. Among the CMIP5 models shown, only CNRM-CM5 indicates negative SMB over the summer months.

Implications of differences in the representation of runoff on predictability are briefly summarized in Table 2, which gives the interannual trends in simulated SMB components. While the reanalysis is forced by satellite and in situ observations, interannual variability in AMIP models is primarily forced with SSTs and trace gas constituents (Gates et al. 1999). Along with the ERA-I, only the GEOS-5 simulations indicate a negative trend in SMB, which is marginally significant in GSN2 over for the integration period. In contrast, the 10 models examined show significant positive trends in SMB, which is generally attributable to increases in the precipitation component. Precipitation trends in the AMIP models are larger than for ERA-I, which is larger than for the GEOS-5 models. The trend in runoff trend is significant and dominates the SMB trend for the ERA-I reanalysis and the GEOS-5 models, while the runoff trend is as large in only a few of the other models.

4. Summary and discussion

A new surface representation for glaciated land surfaces in the GEOS-5 model provides an improved near-surface temperature field and reduces biases in the net surface energy flux as compared to observations. In comparison to in situ AWS observations, a summertime air temperature bias of −4.4°C is reduced to −1.4°C, and significant correction is also found in computed clear-sky surface temperatures in comparison to MODIS-derived values. The scheme eliminates a significant summertime bias in the net surface energy flux in comparison to in situ observations, and an erroneous annual mean net surface energy flux of up to 25 W m^{-2} found in the earlier method. These improvements reveal an underestimate of the surface longwave radiative flux of 4 to 6 W m^{-2} that is compensated for by turbulent fluxes. A downwelling longwave bias is a chronic issue for models in polar regions (e.g., Ettema et al. 2010a) and requires further evaluation, particularly with respect to cloud and aerosol properties.

With the inclusion of a representation of snow hydrology and runoff, the primary variables for SMB are now computed by the GEOS-5 model. Spatial and temporal characteristics of the SMB simulated with a ½° grid spacing compare favorably with results using the RACMO2 and MAR regional climate models, and with historic in situ observations derived from glaciological methods. Simulations of GEOS-5 at 2° grid spacing reproduce principal elements of the SMB field, but lack

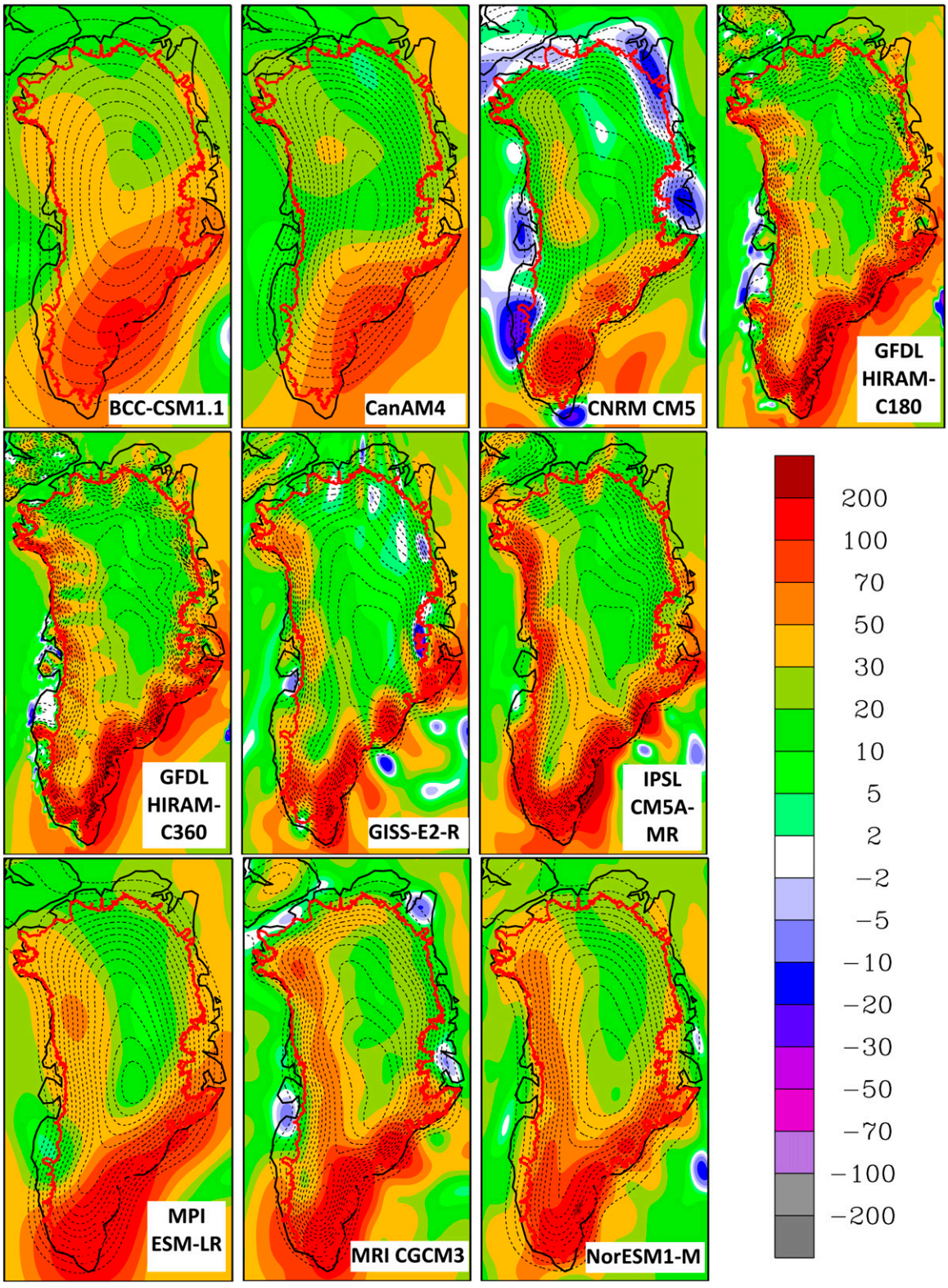

FIG. 12. Annual mean Greenland surface mass balance from ensemble averages of CMIP5 twentieth-century AMIP simulations from 10 models (in cm yr^{-1} w.e.). The average corresponds to the period 1980–2008. The ice sheet margin is indicated with a red line. Topography is signified with dashed contours for every 200 m.

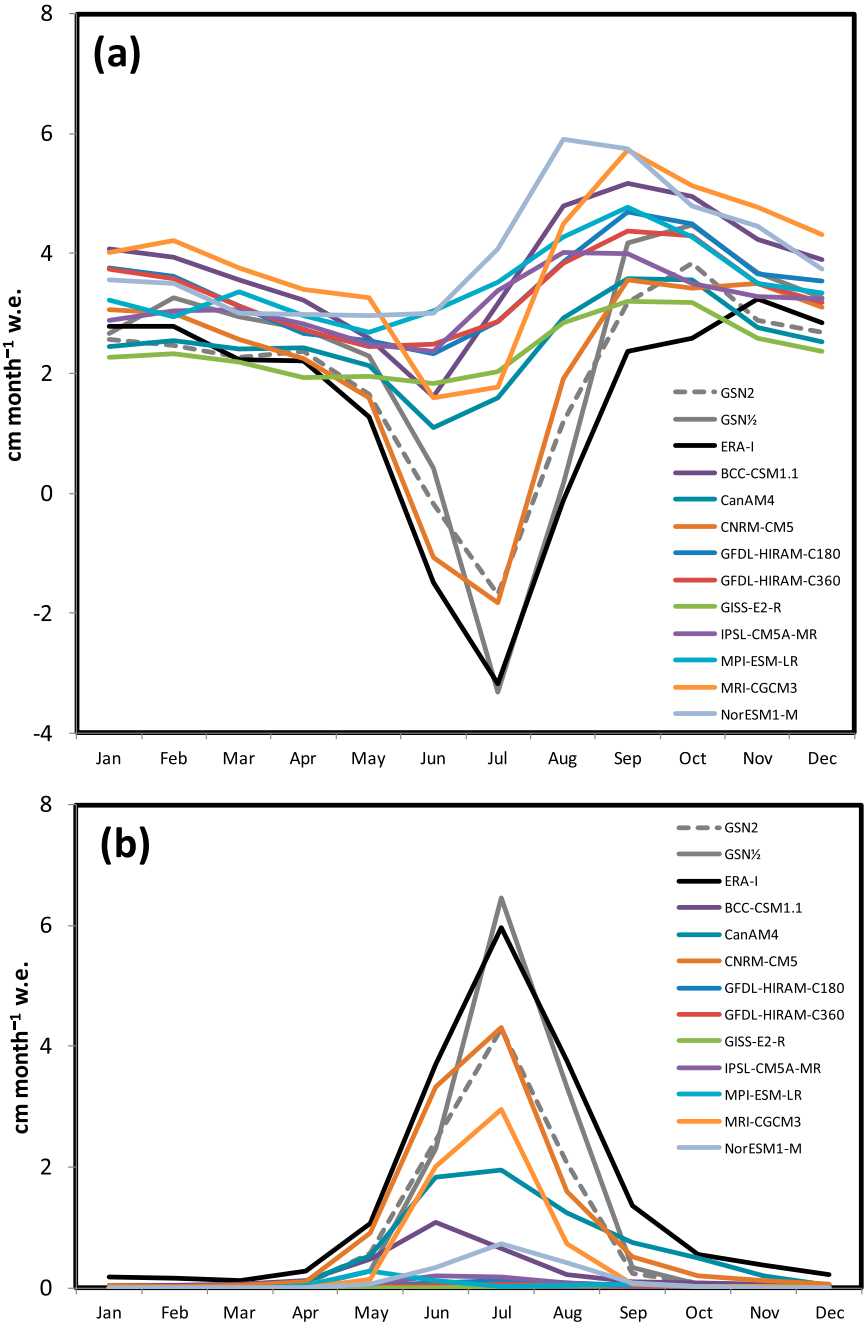

FIG. 13. Monthly (a) surface mass balance and (b) runoff for the GrIS from ensemble averages of CMIP5 twentieth-century AMIP simulations from GEOS-5 at two spatial resolutions, ERA-I reanalysis, and 10 models (in cm yr^{-1} w.e.). The average corresponds to the period 1980–2008.

detailed features of accumulation along the western margins. In comparison to observations, the lower-resolution simulations tend to overestimate the SMB in the southern GrIS by allowing maxima features in accumulation to extend farther inland, while the average SMB over the whole ice sheet is less than that of the ½° simulations. Other contemporary AGCMs examined at resolutions of 2° or coarser also have limited capability in simulating SMB beyond the primary features of large values along the southeastern coast and smaller values to the north and over the interior plateau. This suggests that a grid spacing of greater than 2° or about 200 km is insufficient for adequately resolving coastal accumulation features.

TABLE 2. The trend in SMB components from AMIP simulations of GEOS-5, 10 models of the CMIP5 project for the period 1980–2008, and corresponding reanalysis values from ERA-I (in cm yr^{-1} w.e.). The standard error of the ensemble-averaged trend is indicated in parentheses. Significant trends are shown in bold.

	Ensemble No./grid spacing	*P*	*E*	*R*	SMB
GEOS-5	1/½°				
GSN½ (total)		0.07(0.08)	0.00(0.0)	**0.14(0.05)**	−0.07(0.10)
GSN½ (ice only)		0.07(0.08)	0.00(0.0)	**0.16(0.06)**	−0.09(0.10)
GEOS-5	2/2°				
GSN2 (total)		0.01(0.06)	0.00(0.00)	**0.09(0.02)**	**−0.08(0.06)**
GSN2(ice only)		0.00(0.06)	0.00(0.00)	**0.16(0.03)**	**−0.16(0.07)**
ERA-I	–/0.75°	**0.13(0.07)**	0.00(0.00)	**0.23(0.04)**	**−0.09(0.08)**
BCC-CSM1.1	3/3.6°	**0.16(0.06)**	0.00(0.01)	**0.01(0.00)**	**0.15(0.05)**
CanAM4	4/3.6°	**0.16(0.05)**	−0.01(0.00)	**0.06(0.02)**	**0.11(0.04)**
CNRM-CM5	1/1.875°	**0.29(0.11)**	0.00(0.00)	**0.13(0.04)**	**0.15(0.10)**
GFDL-HIRAM-C180	3/0.5°	**0.17(0.05)**	**0.01(0.00)**	0.00(0.00)	**0.16(0.05)**
GFDL-HIRAM-C360	2/0.25°	**0.23(0.06)**	0.00(0.00)	0.00(0.00)	**0.22(0.06)**
GISS-E2-R	6/2°	**0.17(0.04)**	**0.03(0.01)**	0.00(0.00)	**0.14(0.04)**
IPSL-CM5A-MR	3/1.3°	**0.17(0.06)**	0.00(0.00)	0.00(0.00)	**0.16(0.06)**
MPI-ESM-LR	3/2.5°	**0.18(0.05)**	0.00(0.00)	0.00(0.00)	**0.18(0.05)**
MRI-CGCM3	3/1.5°	**0.19(0.08)**	0.00(0.00)	**0.06(0.01)**	**0.13(0.08)**
NorESM1-M	3/1.875°	**0.20(0.05)**	**0.01(0.00)**	**0.02(0.01)**	**0.18(0.05)**

In comparison to the GEOS-5 model, an analysis of available CMIP5 AMIP simulations finds that only a few models produce significant summertime runoff, a condition that marginally differs from that described by Randall et al. (2007). However, several recent studies have highlighted current work in this area. Using simulations of the GrIS with the Institut Pierre-Simon Laplace (IPSL) global model, Punge et al. (2012) describe the application of a multilevel snow hydrology model that includes compaction processes and prognostic albedo. Vizcaíno et al. (2013) describe the surface configuration for 1° simulations of the CESM coupled model, which include snow hydrologic processes of compaction, percolation, refreezing, and prognostic surface energy computations. Using a downscaling procedure, the CESM was found to compare closely to the RACMO2 regional climate model. The SMB for the CESM plotted at 1° resolution is qualitatively similar to that of the GEOS-5 ½° simulation in showing ablation areas along the western and northern edges of the ice sheet.

Because of the presence of rough topography, spatial resolution is an important factor for adequate simulations of the GrIS. Nevertheless, the treatment of surface hydrological processes is also critical for reproducing the spatial variability and seasonal cycle of SMB. Additional issues of importance include the representation of spatially varying surface albedo, adequate vertical resolution to capture subsurface temperature gradients (Fig. 7), and use of an accurate topography (e.g., Fig. 12; Box and Rinke 2003). An adequate representation of the spatial and temporal characteristics of the surface temperature and SMB over the GrIS are seen as essential for coupling the AGCM with a dynamical ice sheet model. If potential contributions to future eustatic change from polar ice sheets are to be examined with GCMs, then current shortcomings in modeled SMB will need to be remedied.

The surface representation described here will be used in a model coupling strategy to evaluate the relative importance of surface processes versus ice sheet dynamics in the evolution of the GrIS. The scheme is currently being implemented as part of numerical analyses and modeling conducted by the GMAO. Along with a parameterization for sea ice albedo, it will be incorporated as part of a group of improvements for polar processes in the upcoming MERRA2 reanalysis.

Acknowledgments. GC-Net AWS data were obtained from the Cooperative Institute for Research in Environmental Sciences at the University of Colorado at Boulder. DMI AWS data were obtained from the Danish Meteorological Institute. ERA-I fields were obtained from the online ordering system of the European Centre for Medium-Range Weather Forecasts. CMIP5 model output was obtained from the Program for Climate Model Diagnosis and Intercomparison (PCMDI). RACMO2 fields were obtained from the Sea-level Response to Ice Sheet Evolution project (SeaRISE). The authors thank D.K. Hall for access to and assistance in using the MODIS surface temperature dataset. The authors thank C.A. Shuman for constructive suggestions for the revision of the manuscript. Resources supporting this work were provided by the NASA High-End Computing (HEC) Program through the NASA Center for Climate Simulation (NCCS) at Goddard Space Flight Center. This study was funded by a grant from the NASA Modeling Analysis and Prediction Program (MAP) to the second author.

APPENDIX

Expansions of Model Names in Tables 1 and 2

GEOS-5	Goddard Earth Observing System model, version 5
GSN	See text
RACMO2	Royal Netherlands Meteorological Institute's (KNMI's) Regional Atmospheric Model version 2
MAR	Modèle Atmosphérique Régional
ERA-I	Interim European Centre for Medium-Range Weather Forecasts (ECMWF) Re-Analysis
BCC_CSM1.1	Beijing Climate Center, Climate System Model, version 1.1
CanAM4	Atmospheric model from the Fourth Generation Canadian Coupled Global Climate Model
CNRM-CM5	Centre National de Recherches Météorologiques Coupled Global Climate Model, version 5
GFDL-HIRAM-C180	Geophysical Fluid Dynamics Laboratory global High Resolution Atmospheric Model, 180 × 180 grid
GFDL-HIRAM-C360	Geophysical Fluid Dynamics Laboratory global High Resolution Atmospheric Model, 360 × 360 grid
GISS-E2-R	Goddard Institute for Space Studies Model E, coupled with the Russell ocean model
IPSL-CM5A-MR	L'Institut Pierre-Simon Laplace Coupled Model, version 5, coupled with NEMO, mid resolution
MPI-ESM-LR	Max Planck Institute Earth System Model, low resolution
MRI-CGCM3	Meteorological Research Institute Coupled Atmosphere–Ocean General Circulation Model, version 3
NorESM1-M	Norwegian Earth System Model, version 1 (intermediate resolution)

REFERENCES

Agosta, C., V. Favier, G. Krinner, H. Gallée, X. Fettweis, and C. Genthon, 2013: High-resolution modelling of the Antarctic surface mass balance, application for the twentieth, twenty first and twenty second centuries. *Climate Dyn.,* **41,** 3247–3260, doi:10.1007/s00382-013-1903-9.

Alley, R. B., and I. Joughin, 2012: Modeling ice-sheet flow. *Science,* **336,** 551–552, doi:10.1126/science.1220530.

Bales, R. C., J. R. McConnell, E. Mosley-Thompson, and B. Csatho, 2001: Accumulation over the Greenland ice sheet from historical and recent records. *J. Geophys. Res.,* **106,** 33 813–33 825, doi:10.1029/2001JD900153.

——, and Coauthors, 2009: Annual accumulation for Greenland updated using ice core data developed during 2000–2006 and analysis of daily coastal meteorological data. *J. Geophys. Res.,* **114,** D06116, doi:10.1029/2008JD011208.

Bamber, J. L., R. L. Layberry, and S. P. Gogenini, 2001: A new ice thickness and bed data set for the Greenland ice sheet: 1. Measurement, data reduction, and errors. *J. Geophys. Res.,* **106,** 33 773–33 780, doi:10.1029/2001JD900054.

Bengtsson, L., S. Koumoutsaris, and K. Hodges, 2011: Large-scale surface mass balance of ice sheets from a comprehensive atmospheric model. *Surv. Geophys.,* **32,** 459–474, doi:10.1007/s10712-011-9120-8.

Bindoff, N. L., and Coauthors, 2007: Observations: Oceanic climate change and sea level. *Climate Change 2007: The Physical Science Basis,* S. Solomon et al., Eds., Cambridge University Press, 385–432.

——, and Coauthors, 2013: Detection and attribution of climate change: From global to regional. *Climate Change 2013: The Physical Science Basis,* T. F. Stocker et al., Eds., Cambridge University Press, 867–952.

Bindschadler, R. A., and Coauthors, 2013: Ice-sheet model sensitivities to environmental forcing and their use in projecting future sea-level (the SeaRISE project). *J. Glaciol.,* **59,** 195–224, doi:10.3189/2013JoG12J125.

Bougamont, M., J. L. Bamber, and W. Greuell, 2005: A surface mass balance model for the Greenland Ice Sheet. *J. Geophys. Res.,* **110,** F04018, doi:10.1029/2005JF000348.

Box, J. E., and A. Rinke, 2003: Evaluation of Greenland Ice Sheet surface climate in the HIRHAM regional climate model using automatic weather station data. *J. Climate,* **16,** 1302–1319, doi:10.1175/1520-0442-16.9.1302.

Budd, W. F., W. R. Dingle, and U. Radok, 1966: The Byrd Snow Drift Project: Outline and basic results. *Studies in Antarctic Meteorology,* Antarctic Research Series, Vol. 9, M. J. Rubin, Ed., Amer. Geophys. Union, 59–70.

Bugnion, V., and P. H. Stone, 2002: Snowpack model estimates of the mass balance of the Greenland ice sheet and its changes over the twenty-first century. *Climate Dyn.,* **20,** 87–106, doi:10.1007/s00382-002-0240-1.

Carstensen, L. S., and B. V. Jørgensen, 2011: Weather and climate data from Greenland 1958–2010. Danish Meteorological Institute Tech. Rep. 11-10, 22 pp.

Chen, L., O. M. Johannessen, H. Wang, and A. Ohmura, 2011: Accumulation over the Greenland Ice Sheet as represented in reanalysis data. *Adv. Atmos. Sci.,* **28,** 1030–1038, doi:10.1007/s00376-010-0150-9.

Church, J. A., and Coauthors, 2013. Sea level change. *Climate Change 2013: The Physical Science Basis,* T. F. Stocker et al., Eds., Cambridge University Press, 1137–1216.

Cogley, J. G., 2004: Greenland accumulation: An error model. *J. Geophys. Res.,* **109,** D18101, doi:10.1029/2003JD004449.

Cullather, R. I., and M. G. Bosilovich, 2012: The energy budget of the polar atmosphere in MERRA. *J. Climate,* **25,** 5–24, doi:10.1175/2011JCLI4138.1.

Dee, D. P., and Coauthors, 2011: The ERA-Interim reanalysis: Configuration and performance of the data assimilation system. *Quart. J. Roy. Meteor. Soc.,* **137,** 553–597, doi:10.1002/qj.828.

Douville, H., J.-F. Royer, and J.-F. Mahfouf, 1995: A new parameterization for the Météo-France climate model. *Climate Dyn.,* **12,** 37–52, doi:10.1007/BF00208761.

ECMWF, 2007: IFS documentation–Cy31r1. Part IV: Physical processes. ECMWF, 155 pp. [Available online at http://old.ecmwf.int/research/ifsdocs/CY31r1/.]

Ettema, J., M. R. van den Broeke, E. van Meijgaard, W. J. van de Berg, J. L. Bamber, J. E. Box, and R. C. Bales, 2009: Higher surface mass balance of the Greenland ice sheet revealed by high-resolution climate modeling. *Geophys. Res. Lett.,* **36,** L12501, doi:10.1029/2009GL038110.

——, ——, ——, ——, J. E. Box, and K. Steffen, 2010a: Climate of the Greenland ice sheet using a high-resolution climate model—Part 1: Evaluation. *Cryosphere,* **4,** 511–527, doi:10.5194/tc-4-511-2010.

——, ——, ——, and ——, 2010b: Climate of the Greenland ice sheet using a high-resolution climate model—Part 2: Near-surface climate and energy balance. *Cryosphere,* **4,** 529–544, doi:10.5194/tc-4-529-2010.

Farr, T. G., and Coauthors, 2007: The Shuttle Radar Topography Mission. *Rev. Geophys.,* **45,** RG2004, doi:10.1029/2005RG000183.

Fichefet, T., C. Poncin, H. Goosse, P. Huybrechts, I. Janssens, and H. Le Treut, 2003: Implications of changes in freshwater flux from the Greenland ice sheet for the climate of the 21st century. *Geophys. Res. Lett.,* **30,** 1911, doi:10.1029/2003GL017826.

Flato, G., and Coauthors, 2013: Evaluation of climate models. *Climate Change 2013: The Physical Science Basis,* T. F. Stocker et al., Eds., Cambridge University Press, 741–866.

Franco, B., X. Fettweis, C. Lang, and M. Erpicum, 2012: Impact of spatial resolution on the modelling of the Greenland ice sheet surface mass balance between 1990-2010, using the regional climate model MAR. *Cryosphere,* **6,** 695–711, doi:10.5194/tc-6-695-2012.

Gates, W. L., and Coauthors, 1999: An overview of the results of the Atmospheric Model Intercomparison Project (AMIP I). *Bull. Amer. Meteor. Soc.,* **80,** 29–55, doi:10.1175/1520-0477(1999)080<0029:AOOTRO>2.0.CO;2.

Gerdes, R., W. Hurlin, and S. M. Griffies, 2006: Sensitivity of a global ocean model to increased run-off from Greenland. *Ocean Modell.,* **12,** 416–435, doi:10.1016/j.ocemod.2005.08.003.

Glover, R. W., 1999: Influence of spatial resolution and treatment of orography on GCM estimates of the surface mass balance of the Greenland Ice Sheet. *J. Climate,* **12,** 551–563, doi:10.1175/1520-0442(1999)012<0551:IOSRAT>2.0.CO;2.

Greuell, W., and T. Konzelmann, 1994: Numerical modelling of the energy balance and englacial temperature of the Greenland Ice Sheet. Calculations for the ETH-Camp location (West Greenland, 1155 m a.s.l.). *Global Planet. Change,* **9,** 91–114, doi:10.1016/0921-8181(94)90010-8.

Hall, D. K., J. C. Comiso, N. E. DiGirolamo, C. A. Shuman, J. R. Key, and L. S. Koenig, 2012: A satellite-derived climate-quality data record of the clear-sky surface temperature of the Greenland Ice Sheet. *J. Climate,* **25,** 4785–4798, doi:10.1175/JCLI-D-11-00365.1.

Ham, Y.-G., M. M. Rienecker, S. Schubert, J. Marshak, S.-W. Yeh, and S.-C. Yang, 2012a: The decadal modulation of coupled bred vectors. *Geophys. Res. Lett.,* **39,** L20712, doi:10.1029/2012GL053719.

——, S. Schubert, and Y. Chang, 2012b: Optimal initial perturbations for ensemble prediction of the Madden–Julian oscillation during boreal winter. *J. Climate,* **25,** 4932–4945, doi:10.1175/JCLI-D-11-00344.1.

Hanna, E., P. Huybrechts, I. Janssens, J. Cappelen, K. Steffen, and A. Stephens, 2005: Runoff and mass balance of the Greenland ice sheet: 1958–2003. *J. Geophys. Res.,* **110,** D13108, doi:10.1029/2004JD005641.

——, and Coauthors, 2011: Greenland Ice Sheet surface mass balance 1870 to 2010 based on Twentieth Century Reanalysis, and links with global climate forcing. *J. Geophys. Res.,* **116,** D24121, doi:10.1029/2011JD016387.

——, and Coauthors, 2013: Ice-sheet mass balance and climate change. *Nature,* **498,** 51–59, doi:10.1038/nature12238.

Hoch, S. W., 2005: Radiative flux divergence in the surface boundary layer. A study based on observations at Summit, Greenland. Ph.D. dissertation, Swiss Federal Institute of Technology (ETH), Zurich, 164 pp.

Jarosch, A. H., F. S. Anslow, and G. K. C. Clarke, 2012: High-resolution precipitation and temperature downscaling for glacier models. *Climate Dyn.,* **38,** 391–409, doi:10.1007/s00382-010-0949-1.

Koenig, L. S., and D. K. Hall, 2010: Comparison of satellite, thermochron and air temperatures at Summit, Greenland, during the winter of 2008/09. *J. Glaciol.,* **56,** 735–741, doi:10.3189/002214310793146269.

Kojima, K., 1967: Densification of seasonal snow cover. *Proc. Int. Conf. on Low Temperature Science,* Sapporo, Japan, Institute of Low Temperature Science, 929–952.

Koster, R. D., M. J. Suárez, A. Ducharne, M. Stieglitz, and P. Kumar, 2000: A catchment-based approach to modeling land surface processes in a GCM: Part 1. Model structure. *J. Geophys. Res.,* **105,** 24 809–24 822, doi:10.1029/2000JD900327.

Lenaerts, J. T. M., M. R. van den Broeke, J. H. van Angelen, E. van Meijgaard, and S. J. Déry, 2012: Drifting snow climate of the Greenland ice sheet. A study with a regional climate model. *Cryosphere,* **6,** 891–899, doi:10.5194/tc-6-891-2012.

Lin, S.-J., 2004: A vertically Lagrangian finite-volume dynamical core for global models. *Mon. Wea. Rev.,* **132,** 2293–2307, doi:10.1175/1520-0493(2004)132<2293:AVLFDC>2.0.CO;2.

Lipscomb, W. H., and Coauthors, 2013: Implementation and initial evaluation of the Glimmer Community Ice Sheet Model in the Community Earth System Model. *J. Climate,* **26,** 7352–7371, doi:10.1175/JCLI-D-12-00557.1.

Liu, H., K. Jezek, B. Li, and Z. Zhao, 2001: Radarsat Antarctic Mapping Project digital elevation model version 2. National Snow and Ice Data Center, Boulder, CO, digital media. [Available online at http://nsidc.org/data/nsidc-0082.]

Loewe, F., 1970: The transport of snow on ice sheets by wind. *Studies on Drifting Snow,* U. Radok, Ed., Department of Meteorology, University of Melbourne, Publication 13, 1–69.

Loveland, T. R., B. C. Reed, J. F. Brown, D. O. Ohlen, Z. Zhu, L. Yang, and J. W. Merchant, 2000: Development of a global land cover characteristics database and IGBP DISCover from 1 km AVHRR data. *Int. J. Remote Sens.,* **21,** 1303–1330, doi:10.1080/014311600210191.

Lynch-Stieglitz, M., 1994: The development and validation of a simple snow model for the GISS GCM. *J. Climate,* **7,** 1842–1855, doi:10.1175/1520-0442(1994)007<1842:TDAVOA>2.0.CO;2.

Meehl, G. A., and Coauthors, 2007: Global climate projections. *Climate Change 2007: The Physical Science Basis,* S. Solomon et al., Eds., Cambridge University Press, 747–845.

Mernild, S. H., and G. E. Liston, 2012: Greenland freshwater runoff. Part II. Distribution and trends, 1960–2010. *J. Climate,* **25,** 6015–6035, doi:10.1175/JCLI-D-11-00592.1.

Molod, A., L. Takacs, M. Suarez, J. Bacmeister, I.-S. Song, and A. Eichmann, 2012: The GEOS-5 atmospheric general circulation model: Mean climate and development from MERRA to Fortuna. NASA Tech. Rep. NASA/TM-2008-104606, Vol. 28, 115 pp.

Murphy, B. F., I. Marsiat, and P. Valdes, 2002: Atmospheric contributions to the surface mass balance of Greenland in the

HadCM3 atmospheric model. *J. Geophys. Res.,* **107,** 4556, doi:10.1029/2001JD000389.

Nowicki, S., and Coauthors, 2013: Insights into spatial sensitivities of ice mass response to environmental change from the SeaRISE ice sheet modeling project. II: Greenland. *J. Geophys. Res. Earth Surf.,* **118,** 1025–1044, doi:10.1002/jgrf.20076.

Parizek, B. R., and R. B. Alley, 2004: Implications of increased Greenland surface melt under global-warming scenarios: Ice-sheet simulations. *Quat. Sci. Rev.,* **23,** 1013–1027, doi:10.1016/j.quascirev.2003.12.024.

Pollard, D., 2010: A retrospective look at coupled ice sheet–climate modeling. *Climatic Change,* **100,** 173–194, doi:10.1007/s10584-010-9830-9.

Punge, H. J., H. Gallée, M. Kageyama, and G. Krinner, 2012: Modelling snow accumulation on Greenland in Eemian, glacial inception and modern climates in a GCM. *Climate Past,* **8,** 1801–1819, doi:10.5194/cp-8-1801-2012.

Quiquet, A., and Coauthors, 2012: Sensitivity of a Greenland ice sheet model to atmospheric forcing fields. *Cryosphere,* **6,** 999–1018, doi:10.5194/tc-6-999-2012.

Rae, J., and Coauthors, 2011: Twenty-first century climate change in Greenland: A comparative analysis of three regional climate models. Hadley Centre Tech. Note 90, 41 pp.

Randall, D. A., and Coauthors, 2007: Climate models and their evaluation. *Climate Change 2007: The Physical Science Basis,* S. Solomon et al., Eds., Cambridge University Press, 589–662.

Reale, O., W. K. Lau, K.-M. Kim, and E. Brin, 2009: Atlantic tropical cyclogenetic processes during SOP-3 NAMMA in GEOS-5 global data assimilation and forecast system. *J. Atmos. Sci.,* **66,** 3563–3578, doi:10.1175/2009JAS3123.1.

Reijmer, C. H., and J. Oerlemans, 2002: Temporal and spatial variability of the surface energy balance in Dronning Maud Land, East Antarctica. *J. Geophys. Res.,* **107,** 4759, doi:10.1029/2000JD000110.

Reynolds, R. W., N. A. Rayner, T. M. Smith, D. C. Stokes, and W. Wang, 2002: An improved in situ and satellite SST analysis for climate. *J. Climate,* **15,** 1609–1625, doi:10.1175/1520-0442(2002)015<1609:AIISAS>2.0.CO;2.

Ridley, J. K., P. Huybrechts, J. M. Gregory, and J. A. Lowe, 2005: Elimination of the Greenland ice sheet in a high CO_2 climate. *J. Climate,* **18,** 3409–3427, doi:10.1175/JCLI3482.1.

Rienecker, M. M., and Coauthors, 2008: The GEOS-5 Data Assimilation System–Documentation of versions 5.0.1, 5.1.0, and 5.2.0. NASA Tech. Rep. Series on Global Modeling and Data Assimilation, NASA/TM-2008-104606, Vol. 27, 92 pp.

——, and Coauthors, 2011: MERRA: NASA's Modern-Era Retrospective Analysis for Research and Applications. *J. Climate,* **24,** 3624–3648, doi:10.1175/JCLI-D-11-00015.1.

Shepherd, A., and Coauthors, 2012: A reconciled estimate of ice-sheet mass balance. *Science,* **338,** 1183–1189, doi:10.1126/science.1228102.

Slater, A. G., A. J. Pitman, and C. E. Desborough, 1998: The validation of a snow parameterization designed for use in general circulation models. *Int. J. Climatol.,* **18,** 595–617, doi:10.1002/(SICI)1097-0088(199805)18:6<595::AID-JOC275>3.0.CO;2-O.

Smith, I., 1999: Estimating mass balance components of the Greenland ice sheet from a long-term GCM simulation. *Global Planet. Change,* **20,** 19–32, doi:10.1016/S0921-8181(98)00060-5.

Steffen, K., and J. Box, 2001: Surface climatology of Greenland ice sheet: Greenland Climate Network 1995–1999. *J. Geophys. Res.,* **106,** 33 951–33 964, doi:10.1029/2001JD900161.

Stieglitz, M., A. Ducharne, R. D. Koster, and M. J. Suarez, 2001: The impact of detailed snow physics on the simulation of snow cover and subsurface thermodynamics at continental scales. *J. Hydrometeor.,* **2,** 228–242, doi:10.1175/1525-7541(2001)002<0228:TIODSP>2.0.CO;2.

Taylor, K. E., R. J. Stouffer, and G. A. Meehl, 2012: An overview of CMIP5 and the experiment design. *Bull. Amer. Meteor. Soc.,* **93,** 485–498, doi:10.1175/BAMS-D-11-00094.1.

van Angelen, J. H., J. T. M. Lenaerts, S. Lhermitte, X. Fettweis, P. Kuipers Munneke, M. R. van den Broeke, E. van Meijgaard, and C. J. P. P. Smeets, 2012: Sensitivity of Greenland Ice Sheet surface mass balance to surface albedo parameterization. A study with a regional climate model. *Cryosphere,* **6,** 1175–1186, doi:10.5194/tc-6-1175-2012.

van As, D., and R. S. Fausto, 2011: Programme for Monitoring of the Greenland Ice Sheet (PROMICE). First temperature and ablation records. *Geol. Surv. Den. Greenl. Bull.,* **23,** 73–76.

van den Broeke, M., P. Smeets, J. Ettema, and P. Kuipers Munneke, 2008: Surface radiation balance in the ablation zone of the west Greenland ice sheet. *J. Geophys. Res.,* **113,** D13105, doi:10.1029/2007JD009283.

——, and Coauthors, 2009: Partitioning recent Greenland mass loss. *Science,* **326,** 984–986, doi:10.1126/science.1178176.

van de Wal, R. S. W., W. Boot, C. J. P. P. Smeets, H. Snellen, M. R. van den Broeke, and J. Oerlemans, 2012: Twenty-one years of mass balance observations along the K-transect, West Greenland. *Earth Syst. Sci. Data,* **4,** 31–35, doi:10.5194/essd-4-31-2012.

Vaughan, D. G., and Coauthors, 2013. Observations: Cryosphere. *Climate Change 2013: The Physical Science Basis,* T. F. Stocker et al., Eds., Cambridge University Press, 317–382.

Vernon, C. L., J. L. Bamber, J. E. Box, M. R. van den Broeke, X. Fettweis, E. Hanna, and P. Huybrechts, 2013: Surface mass balance model intercomparison for the Greenland ice sheet. *Cryosphere,* **7,** 599–614, doi:10.5194/tc-7-599-2013.

Vizcaíno, M., U. Mikolajewicz, J. Jungclaus, and G. Schurgers, 2010: Climate modification by future ice sheet changes and consequences for ice sheet mass balance. *Climate Dyn.,* **34,** 301–324, doi:10.1007/s00382-009-0591-y.

——, W. Lipscomb, W. Sacks, J. van Angelen, B. Wouters, and M. van den Broeke, 2013: Greenland surface mass balance as simulated by the Community Earth System Model. Part I: Model evaluation and 1850–2005 results. *J. Climate,* **26,** 7793–7812, doi:10.1175/JCLI-D-12-00615.1.

Wientjes, I. G. M., and J. Oerlemans, 2010: An explanation for the dark region in the western melt zone of the Greenland Ice Sheet. *Cryosphere,* **4,** 261–268, doi:10.5194/tc-4-261-2010.

Wild, M., P. Calanca, S. C. Scherrer, and A. Ohmura, 2003: Effects of polar ice sheets on global sea level in high-resolution greenhouse scenarios. *J. Geophys. Res.,* **108,** 4165, doi:10.1029/2002JD002451.

Zwally, H. J., M. B. Giovinetto, M. A. Beckley, and J. L. Saba, 2012: Antarctic and Greenland drainage systems. Cryospheric Sciences Laboratory, NASA Goddard Space Flight Center, Greenbelt, MD, digital media. [Available online at http://icesat4.gsfc.nasa.gov/cryo_data/ant_grn_drainage_systems.php.]